Statistical and systematic errors on kinetic energy of charged particles from the density of nuclear emulsion detector

Phyo Myat Lin
1203921009

DISSERTATION
SUBMITTED TO THE FACULTY OF ENGINEERING,
GRADUATE SCHOOL OF ENGINEERING,
GIFU UNIVERSITY

MARCH 2023

Abstract

Extensive nuclear physics experiments have been performed to investigate the nature of nuclear force between nucleons (*N*-*N*) and baryons (*B*-*B*) from general frameworks. Protons and neutrons, composed of only *u*- and *d*-quarks, are the structural particles of ordinary nuclei. The *N*-*N* interaction has been studied with data from many scattering experiments. On the contrary, hyperons are composed of at least one *s*-quark, and it is not easy to use them as targets or beams for scattering experiments because of their short lifetimes, approximately 10^{-10} s. Therefore, experiments have been conducted to produce hypernuclei, in which hyperons are bound to nuclei. Measurements of the binding energy between the hyperons and the nuclear core can provide information on hyperon-nucleon (*Y*-*N*) interactions. However, the information on hyperon-hyperon (*Y*-*Y*) interactions is very limited because sequential decays take place due to two unit of *s*-quarks, and hypernuclei can travel only a few micrometers in matters from the production to the decay points. For that reason, research on *Y*-*Y* interactions has been conducted by observing double-strangeness hypernuclear events using nuclear emulsion sheets, which have a sub-micrometer spatial resolution.

The interactions on *Y*-*N* and *Y*-*Y*, especially, Ξ-*N* and Λ-Λ, were reported with specific events from the nuclear emulsion experiment (KEK-PS E373), namely KISO and NAGARA events. However, a few events are not sufficient to understand Ξ-*N* and Λ-Λ interactions; thus, the most recent experiment, E07 at J-PARC, was performed to make further investigations by detecting approximately 100 double-strangeness hypernuclei. Currently, 33 events have been observed, and six events among them were already reported.

In the analysis of double hypernuclei, masses of those nuclei were reconstructed by the kinetic energies of decay particles which converted from their ranges. The accuracy of range measurement is one of the main concepts to optimize energy errors. In addition, calibrations of shrinkage factors and densities of emulsion sheets are essential to investigate the statistical and systematical errors in analysis. Shrinkage factors correspond to differences in thickness during beam irradiation and after photo development, and densities correspond to a term to compensate for individual differences in the amount of moisture a sheet contains. Tracks of alpha particles with a monochromatic kinetic energy of 8.785 MeV from ^{212}Po from the

natural radioisotopes of the thorium series have been used as a calibration source to optimize these parameters and range-energy (RE) relation. Although the RE relation between the number of alpha decay events and the error of mass reconstruction is important, it was not sufficiently studied because of a time-consuming method to search for alpha decay events. In the recent past, new methods improved detection and classification efficiency significantly, allowing us to use enormous number of alpha decay events to estimate the corresponding energy error. By utilizing approximately 1500 alpha decay events, the reasonable number of alphas was determined to be at least 150.

On the other hand, the different energetic alpha particles from not only thorium but also uranium series are recorded in the emulsion. In the present analysis of hypernuclear events, only the alpha decay tracks from ^{212}Po of the thorium series are used to calibrate the density of emulsion layer. The range of alpha track from ^{212}Po corresponds to approximately 50 μm in nuclear emulsions; however, the range of hypernucleus can be shorter or longer than 50 μm. Therefore, alpha decay tracks with different monochromatic energies from ^{212}Po were used to evaluate the accuracies of calibrated RE relation for several energy regions.

Systematic uncertainty of the RE relation has been investigated using at least 150 alpha decay tracks for different energies. Alpha decay tracks emitted from ^{8}Be*(2+) state are also used to estimate. Systematic energy error was determined using alpha tracks from ^{212}Po (8.785 MeV), ^{214}Po (7.687 MeV), and ^{226}Ra (4.773 MeV), and the largest systematic energy error between these alpha tracks was estimated to be 25 keV. We have also checked the systematic energy error by applying the calibrated RE to the result of the IBUKI event which was found in the same emulsion sheet. The binding energy error of the IBUKI event was reported to be 0.21 MeV including the systematic or mass error of Ξ^- and daughter nuclei (0.19 MeV) and measurement error (0.8 MeV). The range of ${}^{5}_{\Lambda}$He (87.7 μm) was used to extrapolate the systematic error for the higher energy region, and the affection from the density of the emulsion layer at 87.7 μm was determined to be 22 keV. The result is significantly smaller than the measurement error and shows that the accuracy of the calibration method with alpha particles is reasonable to apply hypernuclear events analysis.

Contents

List of figures

List of tables

CHAPTER 1

1. Introduction

1.1. Hypernuclear physics

Hypernuclear physics is a branch of nuclear physics, and a study of hypernucleus. It is also called as strangeness nuclear physics.

Leptons and hadrons are the two primary classes of elementary particles. Leptons, the lightest particles, are structureless, whereas hadrons, the heavier particles, are made up of two or three quarks. Mesons, which are made up of two quarks, include the pion, kaon, and eta, and baryons, which are made up of three quarks, include the nucleon (*N*) and hyperon (*Y*). There are six different sorts of quarks: up (u), down (d), top (t), bottom (b), strange (s) and charmed (c). An anti-quark exists for each quark. Protons (uud) and neutrons (ddu) are composed of only u- and d- quarks. The nucleus which contains only protons and neutrons is called ordinary nucleus. The hyperon, which contains at least one strange quark such as Λ^0 (uds), Σ^- (dds), Ξ^- (dss) and Ω^- (sss). The nucleus which contains at least one hyperon in addition to nucleon is called strangeness hypernucleus.

One of the main goals of strangeness nuclear physics is to extend our knowledge on the *N*-*N* interaction to the *B*-*B* interaction under SU $(3)_f$ symmetry. The *N*-*N* interaction has been investigated using numerous scattering experiments. The *B*-*B* interaction has received less attention because of the difficulties to detect short-live hypernuclei with scattering experiment while extensive experimental data have been used to study the *N*-*N* interaction. The information on B-B interaction, *Y*-*N* and *Y*-*Y* interaction, can be obtained from the spectroscopic study of hypernuclei.

In 1953, M. Danysz and J. Pniewski discovered the first strangeness -1 hypernucleus using nuclear emulsion exposed to high-energy cosmic rays. The event was considered as a delay disintegration of nuclear fragment containing a Λ^0 hyperon [1]. The delay disintegration of hypernuclear event is shown in Fig. 1.1. This is the beginning of the experimental study of strangeness nuclear physics. The extensive experiments were performed using nuclear emulsion exposed to cosmic rays and later

meson beams from particle accelerators to produce more and more statistics of data samples and various hypernuclei species.

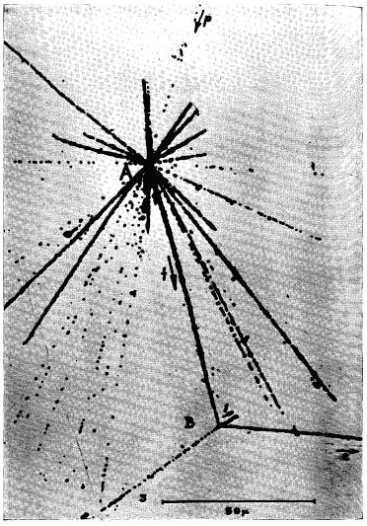

Fig. 1.1 Superimposed image of first decay process of single hypernucleus

1.2. Hypernuclear physics and neutron stars

The neutron stars are the remnants from the supernova explosion. Although the size of neutron star is less than million times of the sun, the mass of neutron star is nearly twice of solar mass. Therefore, they are also known as the smallest and dense stars in the universe. Neutron stars are composed of mainly in neutrons. However, the composition of the interior potion of neutron stars is being observed with the uncertain equation of state (EOS).

Many theoretical estimated results agree that the hyperons may appear in the interior core of neutron stars at the density of 2-3 times of nuclear saturation density [2]. The information of the B-B interaction is quite essential for neutron stars. In order to investigate the information for high density region of neutron stars, we study *Y-N* and *Y-Y* interactions. Since we cannot make the measurement in the neutron stars, we performed the nuclear emulsion experiment that can provide the same information about the interaction between hyperons and nucleons.

1.3. Double hypernuclei

The main purpose of Experiment is to investigate the interaction between baryon-baryon. Nowadays, double-Λ hypernuclei are the best system to investigate the characteristics of the baryon-baryon interaction. Nuclear emulsion technique has been used to studied for over 60 years. E07 experiment is focusing on Ξ-*N* and Λ-Λ interaction strength. The lightest hyperon, Λ, has the mass of 1115.683 MeV/c^2 and it possesses strangeness quantum number S = -1. Λ hyperons which have strangeness quantum number can stay deeply in the nuclear orbit without obeying the Pauli's Exclusion Principle.

The standard notation for a single hypernucleus and double hypernucleus can be denoted as ${}^{A}_{Y}Z$ and ${}^{A}_{YY}Z$, respectively, where Y is the symbol for any embedded hyperon, and Z denotes the electric charge. The mass number *A* stands for the total number of baryons in the system including neutrons, protons, and hyperons. In the case of a helium nucleus (^{4}He), a single and double hypernucleus can be expressed as ${}^{5}_{\Lambda}$He and ${}^{6}_{\Lambda\Lambda}$He, respectively, with the use of Λ hyperon. ${}^{5}_{\Lambda}$He contains two protons, two neutrons and one Λ hyperons while ${}^{6}_{\Lambda\Lambda}$He contains two protons, two neutrons and two Λ hyperons. A nucleus containing one hyperon is called single hypernucleus (S = -1 hypernucleus) and containing two hyperons is called double hypernucleus (S = -2 hypernucleus), respectively.

Double hypernuclei can be produced with a sequential decay process. In order to generate double-Λ hypernuclei, firstly, K^- beam is exposed to the diamond target and then Ξ^- particles are produced by the reaction p (K^-, K^+) Ξ^-. The emitted Ξ^- particle was captured by an atom in emulsion nucleus. Firstly, it is caught in a highly excited atomic orbit and changed into lower orbits by emitting Auger electrons and X-rays. Finally, the nucleus absorbs it, and then it decays into double-Λ hypernuclei, single-Λ hypernuclei, twin single-Λ hypernuclei and others via the reaction; $\Xi^- + p \rightarrow \Lambda + \Lambda + 28$ MeV. The production process is shown in Fig.1.2.

Double-Λ hypernuclei are the best way to understand baryon–baryon interaction, especially, Λ-Λ interaction energy. The mass M $({}^{A}_{\Lambda\Lambda}Z)$ and the binding energy $B_{\Lambda\Lambda}$ $({}^{A}_{\Lambda\Lambda}Z)$ of double-Λ hypernuclei can be experimentally determined by

equation (1.1). Then, the binding energy of two Λ, $\Delta B_{\Lambda\Lambda}$, can be calculated by equation (1.2).

$$B_{\Lambda\Lambda}({}^{A}_{\Lambda\Lambda}Z) = M({}^{A\text{-}2}Z) + 2M(\Lambda) - M({}^{A}_{\Lambda\Lambda}Z) \qquad (1.1)$$

$$\Delta B_{\Lambda\Lambda}({}^{A}_{\Lambda\Lambda}Z) = B_{\Lambda\Lambda}({}^{A}_{\Lambda\Lambda}Z) - 2B_{\Lambda}({}^{A-1}_{\Lambda}Z) \qquad (1.2)$$

The Ξ^- hyperon in an atomic state of a nucleus may interact with the nucleus by Ξ-nucleus interaction. When Ξ^- is captured with emulsion nucleus, twin single-Λ are expected to be produced. The binding energy of Ξ^- hyperon (B_{Ξ^-}) can be known by measuring mass of Ξ^- nucleus. Since the mass of single-Λ hypernuclei are well known from the pest experiments, the mass of Ξ^- nucleus can be estimated from the kinematics. The binding $B_{\Xi^-}({}^{A}_{\Xi}Z)$ can be determined by equation (1.3).

$$B_{\Xi^-}({}^{A}_{\Xi}Z) = M({}^{A\text{-}1}Z{+}1) + M(\Xi^-) - M({}^{A}_{\Xi}Z) \qquad (1.3)$$

Where, $M({}^{A\text{-}1}Z{+}1)$, $M(\Xi^-)$ and $M({}^{A}_{\Xi}Z)$ are the masses of the core nucleus, the Ξ^- hyperon, and the Ξ^--nucleus system, respectively.

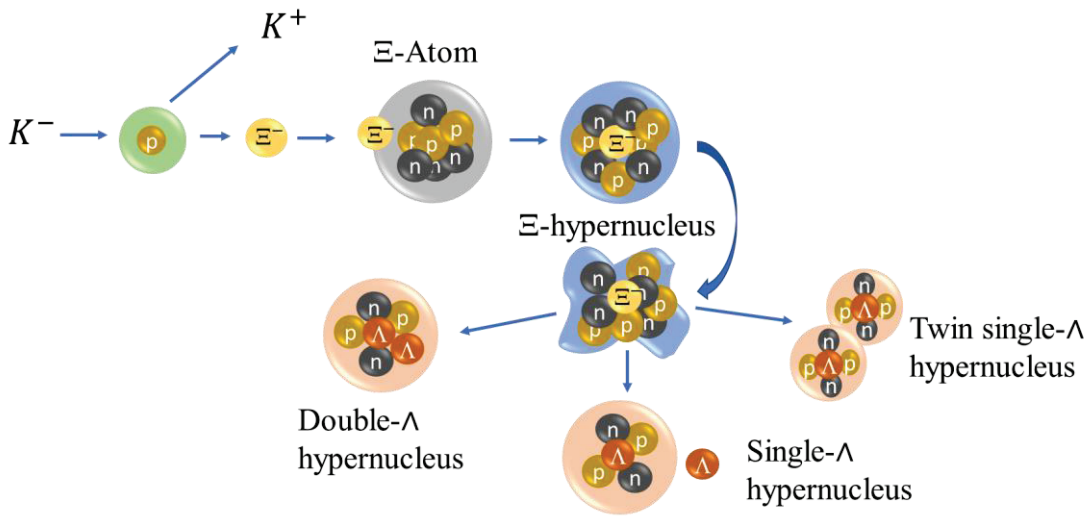

Fig. 1.2 Production process for Λ hypernuclei with the use of quasi free reaction

1.4. Double hypernuclei in the past experiment

In 1963, the first sequential weak decay process of double-Λ hypernucleus produced from a Ξ^- hyperon capture at rest in emulsion was discovered by M. Dyansz

[3]. Subsequent discovery was performed by KEK-PS E176. Among 98 Ξ^- stopped events, four sequential weak decay events of double-Λ hypernuclei were observed by using nuclear emulsion [4]. However, only one event showed the clear track topology of double-Λ hypernucleus in this experiment. Although that event was not uniquely identified, one interpretation for double-Λ hypernucleus was most probable to be ${}^{13}_{\Lambda\Lambda}\mathrm{B}$ [5].

An extensive experiment was conducted by KEK-PS E-373 targeting 10x statistics of the past experiment (E-176). In E-373 experiment, 7 sequential weak decay of double-Λ hypernuclei were observed from nearly 10^3 Ξ^- stopped event. Out of these, four events had clear vertex and track topology. The most remarkable event, NAGARA event, was uniquely identified as ${}^{6}_{\Lambda\Lambda}\mathrm{He}$ nucleus. The value of $\Delta B_{\Lambda\Lambda}$ was determined to be 0.67 ± 0.17 MeV by taking 0.13 MeV of B_{Ξ^-} [6]. ${}^{6}_{\Lambda\Lambda}\mathrm{He}$ nucleus gave the information of the first evidence of attractive Λ-Λ interaction energy. In this experiment, a twin single-Λ hypernucleus, namely KISO event which show that the first evidence of deeply bound state of the Ξ^--nucleus system, was also found [7,8]. Only a few events are not sufficient to prove the Ξ^--nucleus and Λ-Λ interaction energies. Thus, further investigation is needed to claim the double-Λ hypernucleus with minimal uncertainty.

Following from these, JPARC-E07 was performed to investigate more effective double hypernuclei by increasing ten times statistics of past experiment, E-373.

1.5. Objective

The calibration of density of emulsion layer is very important for the analysis of hypernuclear events in the nuclear emulsion experiment. However, the statistical and systematic error from the density calibration was not sufficiently studied yet. Therefore, the purpose of this research is to estimate the statistical and systematic energy errors which come from the density of emulsion layer.

CHAPTER 2

2. Experimental study of double hypernuclei

E07 experiment was performed with an upgraded counter-emulsion hybrid method in order to detect 10 times statistic of the past experiment [9]. In order to detect more double hypernuclei, the great amount of Ξ^- stop events in nuclear emulsion are needed than that of E373 experiment. In this experiment, 2.1 tons of emulsion gel was used to produce a large amount of emulsion sheets, which is 3 times quantities of E373 experiment.

2.1. Experimental setup for E07 experiment

The K^- 1.8 beam line is used in JPAC E07 experiment. K^- beam with momentum of 1.8 GeV/c were radiated to the diamond target and Ξ^- particles were created via the quasi-free reaction, $K^- + p \longrightarrow \Xi^- + K^+$. A typical beam intensity was 3 x 10^5 per spill with the time of 2 seconds. Beam line spectrometer was used to detect the momentum of incoming kaon beam. A diamond target with the size of 50.6 mm wide, 30.3 mm high and 30.4 mm thick was placed upstream of emulsion stack. It is used not only the Ξ^- production target but also the energy degrader of Ξ^- hyperon. Some of Ξ^- hyperon from the diamond target came to rest in nuclear emulsion stack to produce double strangeness hypernuclei. KURAMA spectrometer which contains KURAMA magnet, four trigger counters (PVAC, FAC, SCH, TOF) and five tracking detectors (SSD1, SSD2, SDC1, SDC2, AND SDC3) was used to detect the momentum of outgoing particles. Two sets of high precision position tracking detector, silicon strip detectors (SSD) were placed between the target and the nuclear emulsion detector to obtain the precise angle and position information of the track of incoming Ξ^- hyperon. In addition, another two sets of SSD were set in the back side of emulsion stack to obtain the angle and position of the scattered particles from nuclear emulsion. The germanium (Ge) detector, called Hyperball-X was used to measure X-ray of Ξ^- atom. A schematic drawing of experimental setups near the emulsion stack are shown in Fig.2.1. The detail explanation of experimental setup for E07 experiment was expressed in [10] and [11].

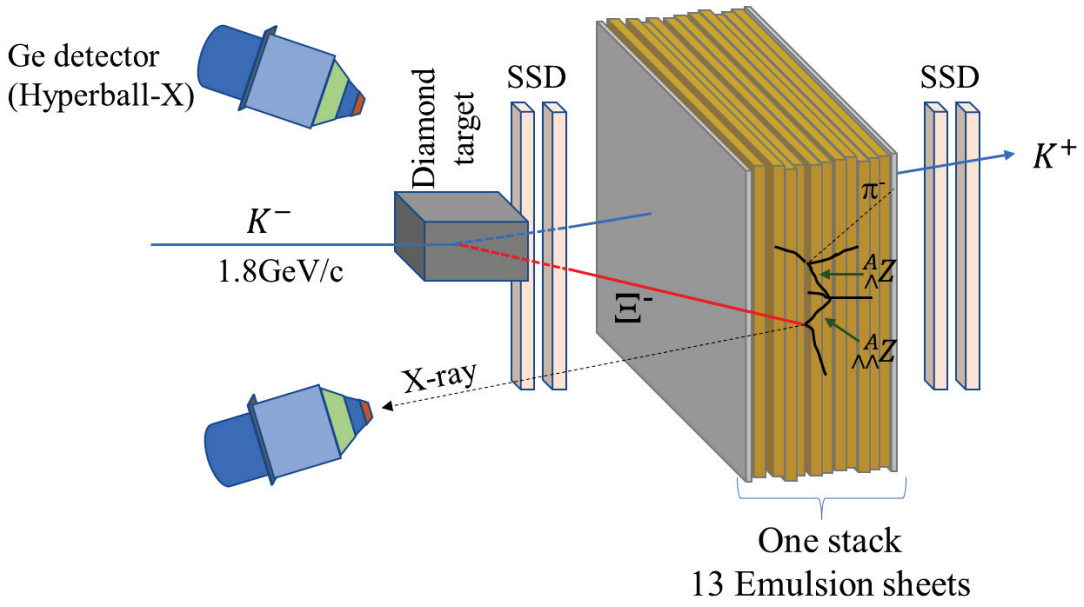

Fig. 2.1 Experimental setup for E07 experiment around nuclear emulsion stack

2.2. Nuclear emulsion detector

The use of nuclear emulsions has a long history in high energy particle physics. In 1910, Japanese scientist, S. Kinoshita used nuclear emulsion detector for the first time to demonstrate that the silver halide grains can be developed in emulsion by using recorded single alpha particle. In the earlier days, nuclear emulsions were not sensitive to high velocity single charged particles. In the end of 1940, C. F. Powell, Occhialini and their collaborators made the emulsions to have more sensitive for singly charged particles by increasing the content of silver bromide and made the emulsion thicker by increasing the active volume in order to record the tracks of less ionizing-faster-particles. In 1947, C. F. Powell found the track of charged particle can be recorded in emulsion even if the particles' velocity is closed to the velocity of light [12]. Nuclear emulsion has a very large sensitivity to all charged particle and large density detector that made its role very important in studying of high energy physics. Therefore, emulsion detector is one of the best among the various particle detectors to study of the production and decay of short-lived particles.

2.3. Photographic development

The study of hypernuclei have been carried out using the emulsion technique. Nuclear emulsion is the only detector which has a position resolution of 1 μm and the best three-dimensional charged particles detector. Nuclear emulsion is a compound solid detector which is made up of mainly in emulsion gel with interspersed silver bromide (AgBr) crystal and other materials. The AgBr crystal in the emulsion are sensitive to the passage of ionizing charge particles.

When a charged particle passed through to nuclear emulsion, the energy released by ionizing particles to the AgBr crystal produce latent images. These latent images can be seen like a serial black silver grains by using two chemical treatment process, called development, and fixing. Because of the passage of charged particle, a sequence of silver grains can be defined as a track. In principle, nuclear emulsion is same as ordinary photographic film. The difference is only two: larger thickness and higher sensitivity of nuclear emulsion than photographic film. That make sense to study the interaction of high energy particles, which has minimum ionization power.

The effect of ionizing cosmic radiation to the nuclear emulsion can cause the formation of latent images. Cancellation of latent image is called fading. In order to delete unwanted tracks which is caused by cosmic radiation recorded in the emulsion during stocking or transportation, fading process can be applied by setting the high temperature and humidity. The process of transforming the latent image into a cluster of visible images by chemical treatment process is called photographic development. After photographic development the paths of charged particles are recorded as 3-dimensional sequence of the silver grains in the emulsion. These grains have a micrometric size, and it can be seen with optical microscope. The purpose of chemical treatment process is to maximize the developed silver grains which possess the latent image and to minimize an accidentally developed grains of other crystal due to thermal excitation. Fixing process is applied to remove all the residual crystal in emulsion. Fig. 2.2 show the process of image formation in nuclear emulsion.

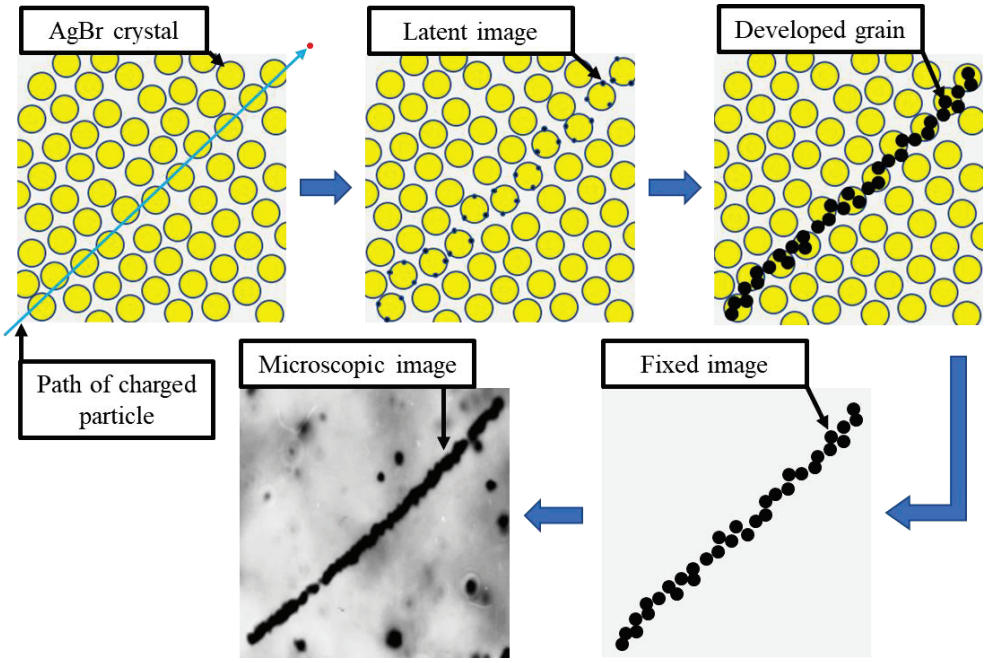

Fig. 2.2 Photographic development process in nuclear emulsion

After treatment process, however, although the area of nuclear emulsion is not significantly deformed due to the providence of polystyrene base film, the thickness of emulsion is shrunk to nearly one half of original thickness as shown in Fig. 2.3. To get the optimal Range-Energy relation of charged particles, we must recreate their initial range while accounting for emulsion layer shrinkage due to photographic processing. Since the density of emulsion depends on the water content and shrinkage factor, the Range-Energy relation should be calibrated by the shrinkage factor and emulsion density. Alpha particles from natural radio isotopes has been used for density calibration for more than 50 years. The detail of Range-Energy calibration method and density calibration methods will be described in chapter 3 and chapter 4.

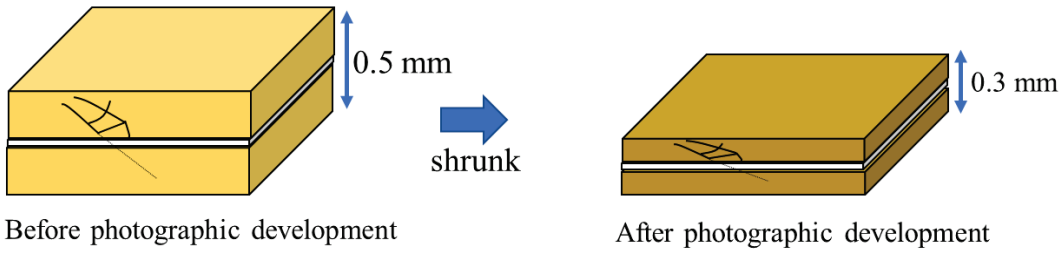

Fig. 2.3 The effect of photographic development on nuclear emulsion to Range-Energy relation

2.4. Nuclear emulsion for the E07 experiment

Fuji GIF emulsion gel was used for E07 emulsion production. The size of AgBr in Fuji GIF emulsion was 0.2 μm. The composition of all elements in Fuji GIF emulsion are listed in table.2.1 [13]. Emulsion plates are fabricated by pouring emulsion gel on one side of polystyrene base film at first. After drying emulsion gel, another side of base film are poured by emulsion gel and dried again. Base film was used to maintain the original size of the nuclear emulsion during the process of drying, developing and for long term stoking. Base film is not sensitive to charged particles.

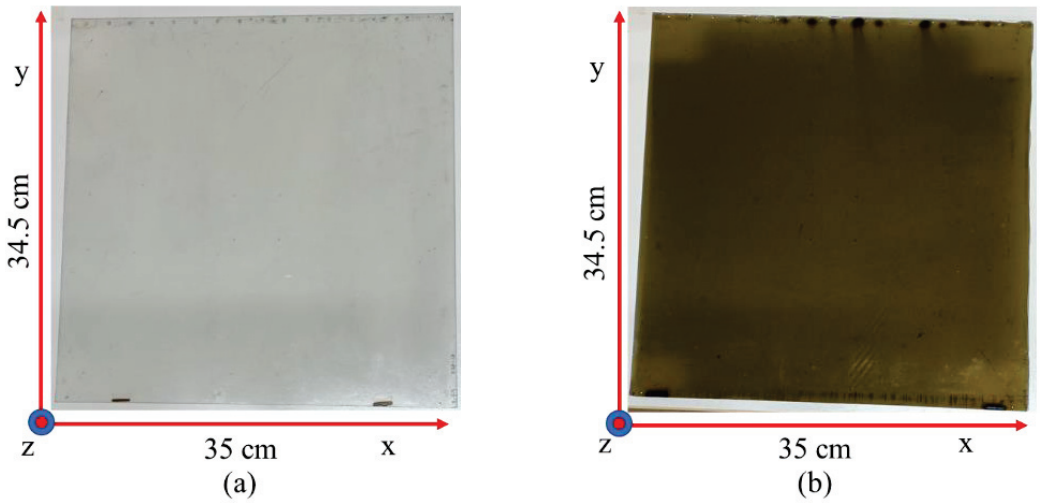

Fig. 2.4 Photographic nuclear emulsion for E07 experiment (a) thin-type emulsion and (b) thick type emulsion

Table 2-1 Design value of the composition of all elements in Fuji GIF emulsion

Materials	Density [g/cm3]
H	0.05
C	0.326
N	0.11
O	0.23
Br	1.166
Ag	1.6
I	0.033
others	0.05

Two types of emulsion plates are used in E07 experiment, thin-type and thick-type with the area of 35 x 34.5 cm^2 as shown in Fig.2.4 (a) and (b). One module or one emulsion stack consist of 2 thin-type sheets and 11 thick-type sheets. The thin-type sheet is composed of 100 μm of emulsion layer on both sides of 180 μm of polystyrene base film while the thick-type sheet is composed of 450 μm of emulsion layer on both sides of 40 μm of polystyrene base film. The first most and the last most sheets of emulsion stack were set thin-type emulsion sheets. Fig.2.5. illustrate the stack structure for E07 experiment. The first most thin-type emulsion was used to connect Ξ^- tract from SSD 1. The last most thin-type emulsion was used to connect the track to SSD 2 if the decay daughter particles of hypernucleus through the emulsion stack. Thick-type emulsion are used for Ξ^- capture and tracking. 118 modules were exposed to beam with the amount of 236 thin-type and 1238 thick-type emulsion sheets.

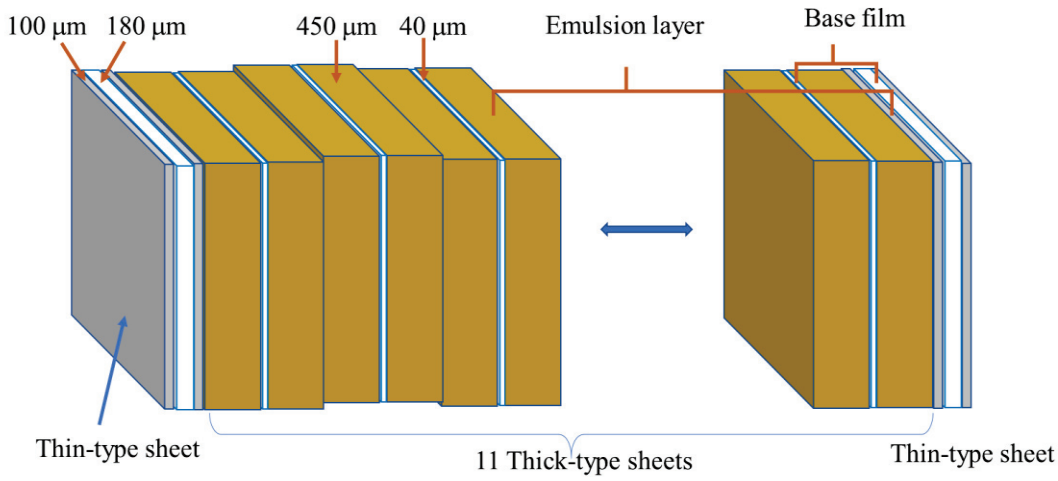

Fig. 2.5 Illustration of emulsion stack position for E07 experiment during beam exposure

2.5. Event classification in nuclear emulsion

Using the predicted position and angle of Ξ^- hyperon from SSD 1, Ξ^- tracks are scanned in the first most thin-type emulsion by microscopic scanning system. The detected Ξ^- tracks are automatically traced through several emulsion sheets. When the Ξ^- stopping point is detected, the system automatically record the track. Then the stopping points are checked by human eyes where they really stop or through. Based

on the mechanism of Ξ^- stop in the nuclear emulsion, several types of stop events can be categorized as follow and the track topologies are shown in Fig.2.6.

σ-stop: The followed Ξ^- track stop in nuclear emulsion and emit at least one charged particle. The σ-stop event can be distinguished from other stop events by seeing thickness and dizzy track near stop point. Moreover, hypernuclear events like single-Λ, twin single-Λ and double-Λ hypernuclei can be categorized as in σ-stop.

ρ-stop: If a track dizzily stopped in emulsion without any other decay track, it is called ρ-stop.

Decay: If the incoming particle decay into one visible thin tack and invisible neutral particle, it can be noted as decay event.

Beam interaction: If K^- beam directly enter into the nuclear emulsion and interact with emulsion nucleus, a reaction vertex is formed with several tracks. When a beam track located in the normal direction to the upstream of vertex position, the event is interpreted as beam interaction.

Secondary interaction: Secondary interaction is the in-flight interaction between Ξ^- and emulsion nucleus.

Through: The followed track escaped from the emulsion stack without interacting with emulsion nucleus or without decaying.

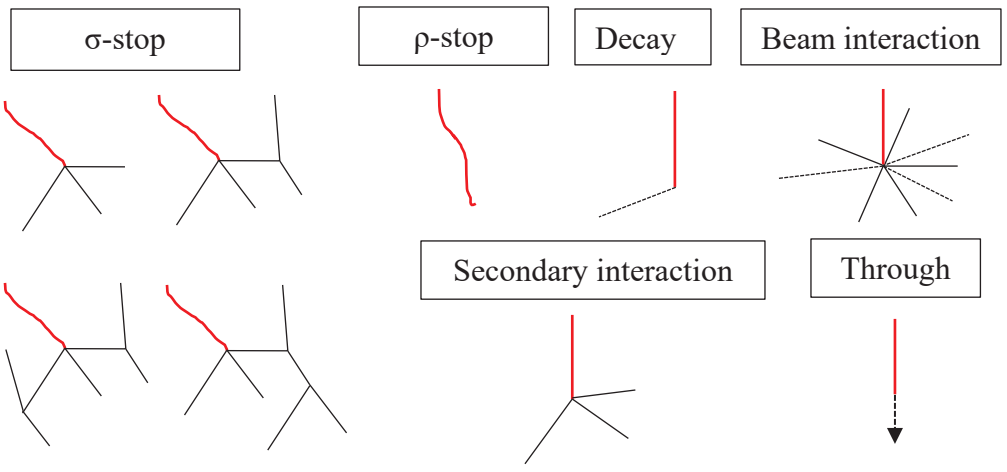

Fig. 2.6 Schematic drawing of event topologies after following the candidates of Ξ^- track in nuclear emulsion sheet. The red color represents the incoming track.

2.6. Detected double hypernuclei from E07 experiment

From the E373 experiments, only two events were uniquely identified as double-Λ hypernucleus and twin single-Λ hypernucleus. The two events show that the attractive Λ-Λ interaction energy and the deeply bound state of the Ξ^--nucleus system. The E373 experiments has opened the door of S = -2 hypernuclear physics. However, it is crucial to achieve more uniquely identified event in order to obtain the knowledge of Λ-Λ and Ξ-*N* interactions without any ambiguity arising from the different core nuclei.

Following from the past experiment, therefore, JPARC-E07 was performed to investigate more effective double-Λ hypernuclei by increasing ten times statistics of past experiment, E-373. This experiment was aimed to detect 100 double hypernuclei by stopping nearly 10^4 Ξ^- . So far, 33 double hypernuclear events have been detected after the first period analysis scheme of E07 experiment. Fig. 2.7 Shows the superimposed image of detected double hypernuclear event from E07 experiment.

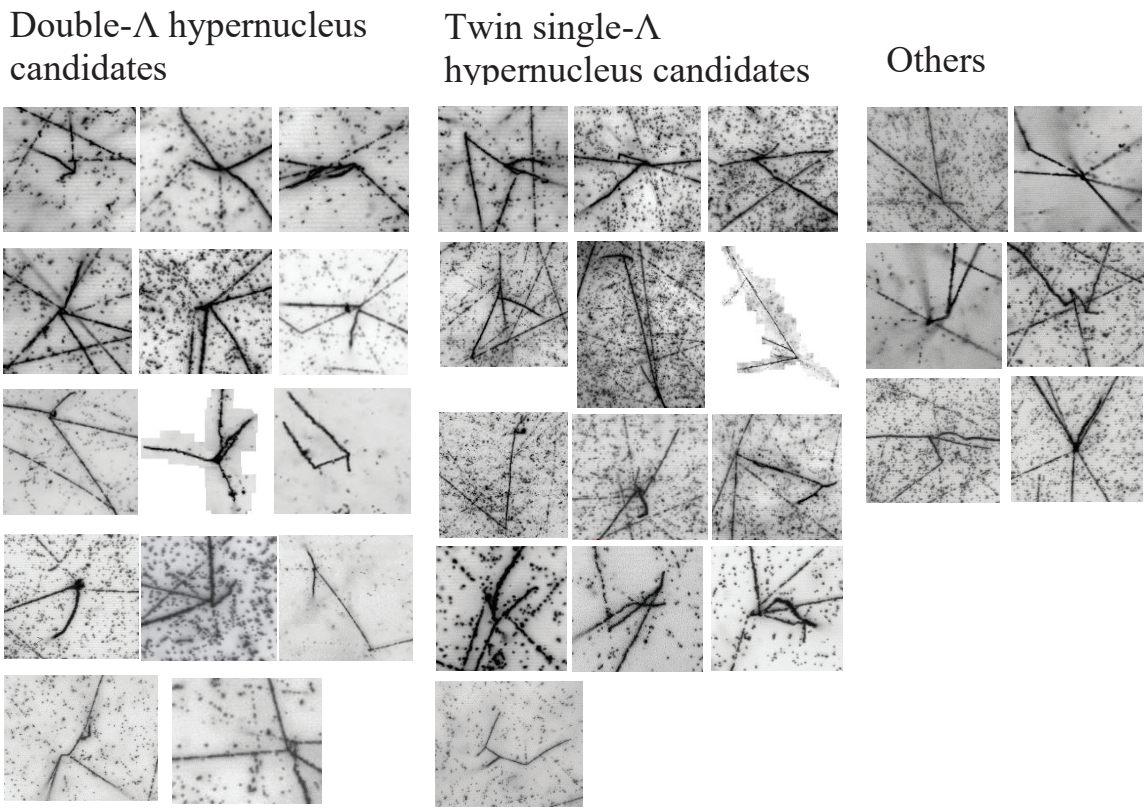

Fig. 2.7 The candidates of detected double hypernuclear events from J-PARC E07 experiment

Among them, two events of double-Λ hypernuclei, namely as MINO and D001, were analyzed and published. MINO event was interpreted with possible candidates as [14]

$$\Xi^- + {}^{16}\mathrm{O} \rightarrow ({}^{10}_{\Lambda\Lambda}\mathrm{Be}, {}^{11}_{\Lambda\Lambda}\mathrm{Be}, {}^{12}_{\Lambda\Lambda}\mathrm{Be}) + {}^{4}\mathrm{He} + (\mathrm{t}, \mathrm{d}, \mathrm{p})$$

$B_{\Lambda\Lambda}$ ($\Delta B_{\Lambda\Lambda}$) for the candidates were obtained as 15.05 ± 0.11 MeV (1.63 ± 0.14), 19.07 ± 0.11 MeV (1.87 ± 0.37), and 13.68 ± 0.11 MeV (-2.7 ± 1.0 MeV), respectively. The most probable double-Λ hypernucleus was interpreted as ${}^{11}_{\Lambda\Lambda}\mathrm{Be}$ based on the kinematic fitting result.

The D001 event was interpreted as [15]

$$\Xi^- + {}^{14}\mathrm{N} \rightarrow {}^{10}_{\Lambda\Lambda}\mathrm{Be} + {}^{4}\mathrm{He} + \mathrm{n}$$

$B_{\Lambda\Lambda}$ and $\Delta B_{\Lambda\Lambda}$ for the D001 event was determined as 15.22 ± 2.78 MeV and 1.80 ± 2.78 MeV, respectively. The Λ-Λ interaction energy of D001 event agrees with NAGARA and MINO events.

Moreover, twin single-Λ hypernuclear events; IBUKI [16], IRRAWADDY [17], T007 [17], and T011 [17] were also reported. Among them, IBUKI and IRRAWADDY events are uniquely identified, and their results are consistent with the theoretical calculation. The production and the decay modes of IBUKI event was interpreted as

$$\Xi^- + {}^{14}\mathrm{N} \rightarrow {}^{15}_{\Xi}\mathrm{C} \rightarrow {}^{10}_{\Lambda}\mathrm{Be} + {}^{5}_{\Lambda}\mathrm{He}$$

The binding energy of Ξ^- hyperon in the Ξ-^{14}N system (B_{Ξ^-}) was determined to be 1.27 $\pm$ 0.21 MeV. The result indicates that the Ξ-^{14}N was bound system and it is consistent with the nuclear 1p state of theoretical calculation results.

In the case of IRRAWADDY event, the reaction process of Ξ-^{14}N system was obtained as

$$\Xi^- + {}^{14}\mathrm{N} \rightarrow {}^{15}_{\Xi}\mathrm{C} \rightarrow {}^{5}_{\Lambda}\mathrm{He} + {}^{5}_{\Lambda}\mathrm{He} + {}^{4}\mathrm{He} + \mathrm{n}$$

The B_{Ξ^-} of IRRAWADDY event was determined to be 6.27 ± 0.33 MeV. The B_{Ξ^-} value represent a deeply bound state of Ξ-^{14}N system. The bound state is consistent with the nuclear 1s of theoretical calculation results. Fig. 2.8 show the B_{Ξ^-} of twin single-Λ hypernuclei observed in the past and current experiment. By considering the

experimental and theoretical predictions, the binding energies level of Ξ^- hyperon in IBUKI and IRRAWADDY events will be the first evidence of the nuclear 1p and 1s states.

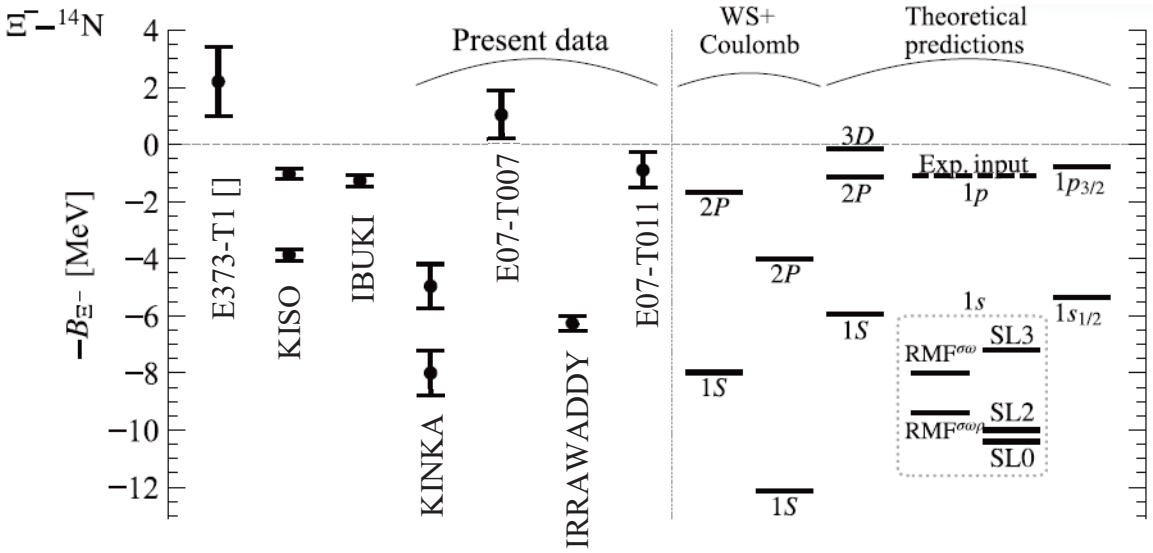

Fig. 2.8 The graph of B_{Ξ^-} for the detected twin single-Λ hypernuclei and theoretical predictions. The figure was taken from ref. [17]

CHAPTER 3

3. Analysis methods

3.1. Range-energy (RE) relation

To calculate the Ξ-N and Λ-Λ interactions, it is necessary to know the mass of double hypernuclei. The mass can be obtained by measuring the kinetic energy (*KE*) at the decay of daughter particles. The *KE* is converted from the range of charged particles in the emulsion sheet by the following range−energy (RE) relation [17]:

$$R = \frac{M}{Z^2} . \lambda(\beta) + MZ^{\frac{2}{3}} C_z \left(\frac{\beta}{Z}\right) \quad (3.1)$$

where *R* and *Z* represent the range and charge of particles, respectively. *M* is the mass of charged particles in proton mass units. C_z is an empirical function to correct range extension, which was experimentally estimated as a function of $\frac{\beta}{Z}$ for various nuclei. In this case, $\lambda(\beta)$ is the range of protons at velocity βc in the emulsion layer of the E07 experiment, which is expressed as [18]

$$\frac{\lambda_s}{\lambda(\beta)} = \frac{rd-1}{rd_s-1} + \frac{r(d_s-d)}{rd_s-1} . \frac{\lambda_s}{\lambda_w} \quad (3.2)$$

where λ_s and λ_w are proton ranges in the standard emulsion layer and water, respectively. Further, d_s and d are the densities of the standard emulsion layer (3.815 g.cm^{-3}) and the emulsion layer used in the current experiment, respectively; r is the ratio increment of the volume to weight caused by the absorption of moisture in the emulsion layer.

3.2. RE relation and mass error of hypernuclei

A nuclear emulsion sheet is made up of emulsion gel with a dispersion of silver halide crystal and polystyrene film base. To visualize the tracks of charged particles in the emulsion sheet under microscopes, a photographic development was performed after beam exposure. In the development process, a fixation process to remove undeveloped silver halide was also applied in order to prevent image degradation. After photographic development, the thickness of emulsion layer was reduced to nearly one-half of the original thickness due to the removal of silver halide, which can be

represented as shrinkage factor (S). Therefore, the calibration of the shrinkage factor and the density of emulsion layer by the use of alpha tracks of several tens number in each emulsion sheet is important to get the optimal RE relation. Alpha tracks from the natural radioisotopes of the thorium series and uranium series have been used as energy−calibration sources to calibrate the density change of emulsion layers for the last half-century. Although the relation between the number of alpha decay events and the error of mass reconstruction is important, it has not been sufficiently studied.

On measuring the range of charged particles in the nuclear emulsion sheet, an error called range straggling arises and affects the mass error of the double hypernucleus. This error of range straggling (ΔR) is a statistical error, and it can be calculated by the following equation as a function of KE [19]:

$$\Delta R\ (KE) = \frac{\sqrt{M}}{Z^2}\ .\Delta R_p\ \left(\frac{KE}{M}\right) \tag{3.3}$$

where ΔR_p represents the error of range straggling by the proton. The KE and kinetic energy error (KE_{err}) from density error of emulsion layer (d_{err}) and error of range straggling will be described in a later part of this paper.

There are many alpha decay tracks from thorium and uranium series in the emulsion. However, in the present analysis of hypernuclear events from E07 experiment, alpha track from ^{212}Po of thorium series, which have monochromatic energy of 8.785 MeV were used to calibrate the density of emulsion layer. The density of emulsion layer should be uniform in one emulsion sheet. The track of charged particles may change depend on the density of emulsion layer. If the density is changed, the kinetic energy which converted from the range of charged particles will also be changed and it will distribute to the mass error of double hypernuclei. Recently, E. Liu et.al reported the systematic energy error from the density of emulsion layer was to be approximately 28 keV using Monte Carlo simulation [20]. We should investigate systematic energy error for every hypernucleus of E07 experiment using current experimental data taken from E07 emulsion.

Therefore, the purpose of this research is to investigate the statistical and systematic energy errors which derived from the density of emulsion layer in order to minimize the mass error of hypernuclei. The next chapter will be described how to calculate statistical and systematic energy error.

3.3. Characteristics of natural radioisotopes in nuclear emulsion

The long decay chain of naturally radioactive elements results in an alpha decay when a parent nucleus disintegrates into a daughter nucleus. Most of natural radio isotopes decay through the emission of alpha and beta until they got a stable state of nucleus. Nuclear emulsion can record 3-dimentional track of decay alpha particles which is naturally occur in air during the time from emulsion production and until photographic development.

Since the emulsion stocking time between emulsion production and beam exposure is nearly two years, it has enough time to record 4 alpha decay tracks from uranium series and 5 alpha decay tracks from thorium series. The decay chain and superimposed images of natural radioisotopes in the emulsion sheet are shown in Fig. 3.1 and Fig.3.2.

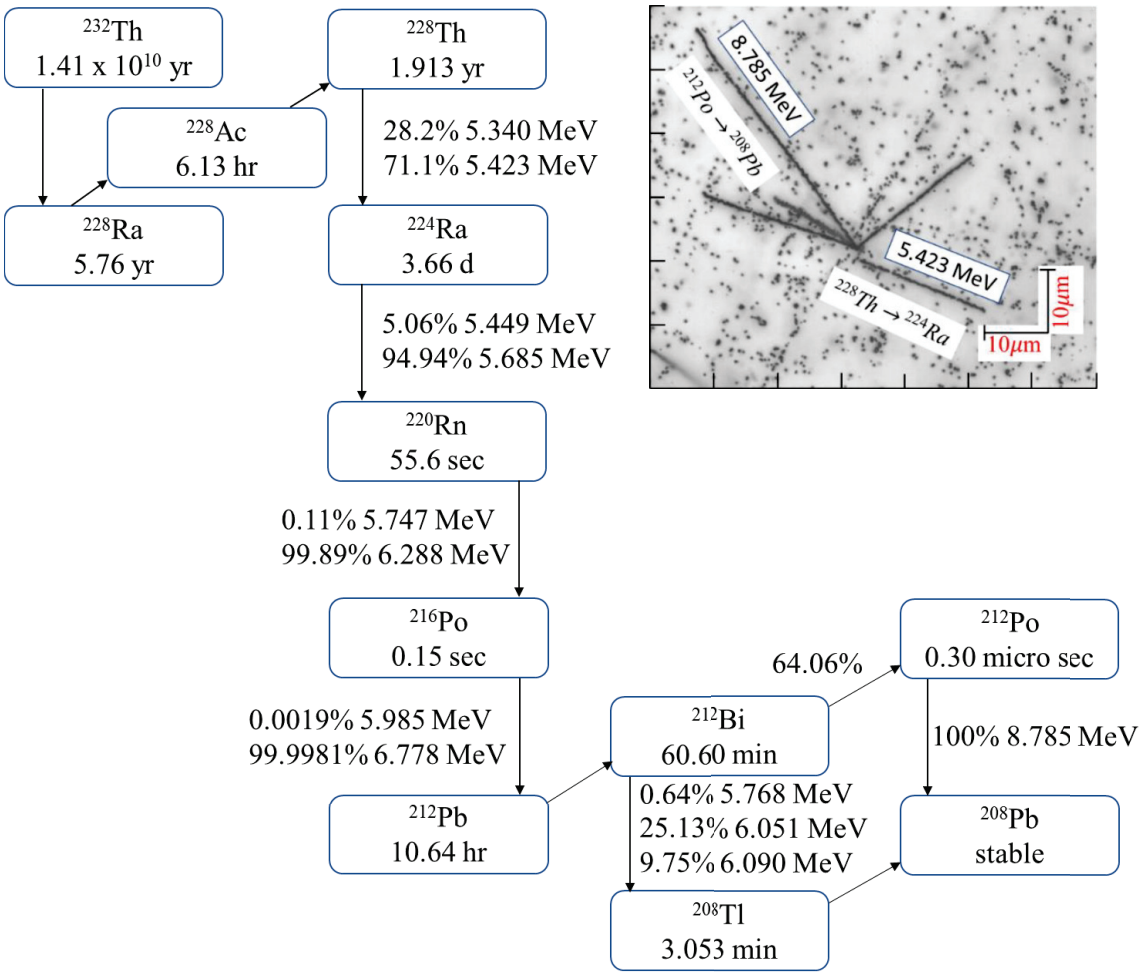

Fig. 3.1 Decay chain and superimpose images of alpha decay tracks from thorium in the emulsion

In thorium decay chain, alpha decay track from ^{212}Po has the highest energy of 8.785 MeV. In uranium decay chain, alpha decay track from ^{214}Po has the highest energy of 7.687 MeV. These tracks can be seen as the longest track among the decay tracks and can be easily discriminated from other decay track. Alpha decay track from ^{224}Ra in uranium series and alpha decay track from ^{222}Rn in uranium series may move with thermal motion in emulsion during their lifetime of 3.63 and 3.82 days, respectively. Therefore, most of alpha decay tracks from ^{228}Th and ^{226}Ra can be seen separately from other decay tracks due to lifetime of ^{224}Ra and ^{222}Rn, respectively. Each of alpha decay tracks from thorium and uranium series have their respective energies.

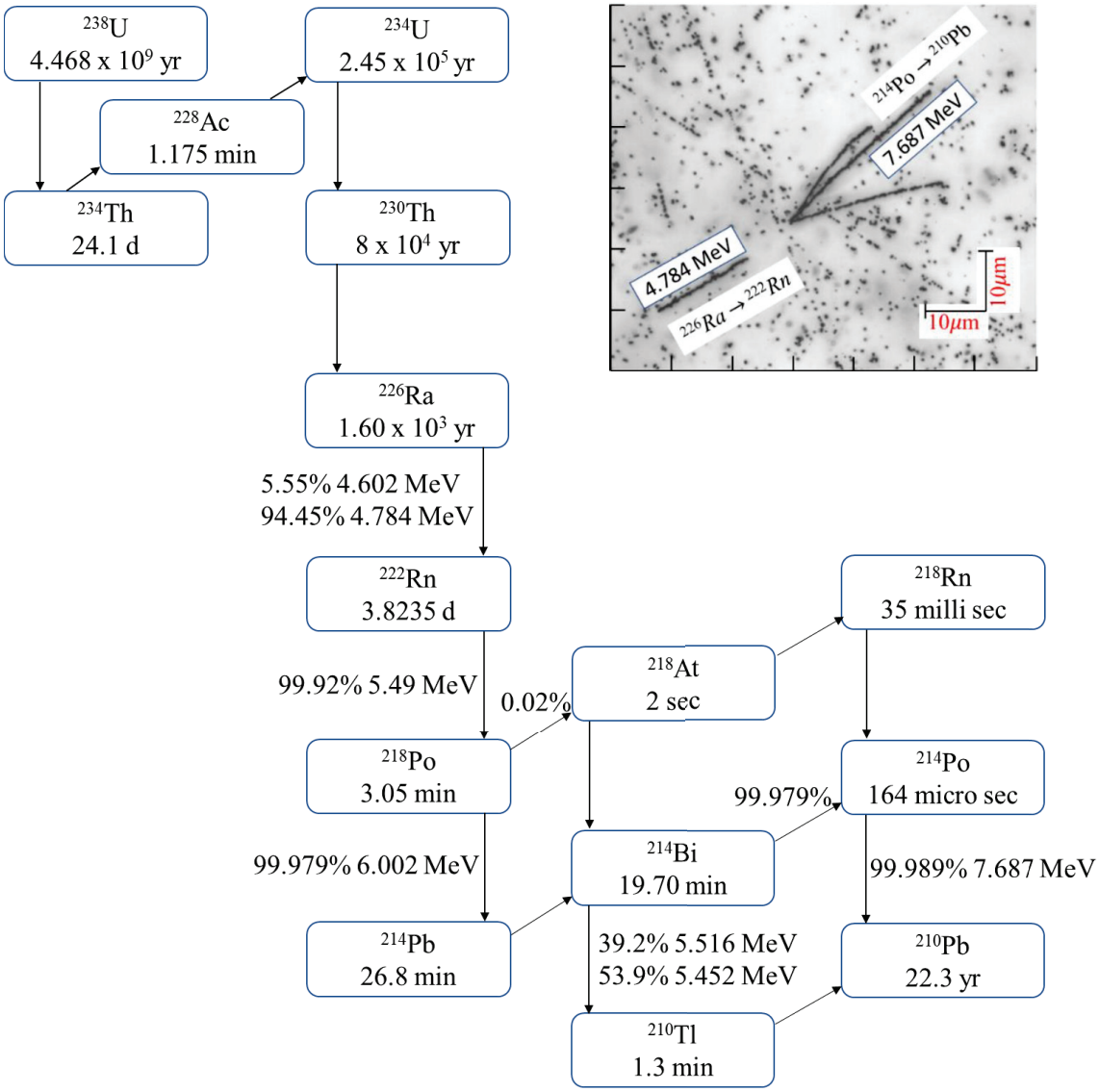

Fig. 3.2 Decay chain and superimpose images of alpha decay tracks from uranium in the emulsion

3.4. Hammer track event

Hammer track was first reported by Occhialini and Powell, and it was estimated to be due to β decay of ^{8}Li fragment which comes from nuclear disintegration [21]. ^{8}Li decay with the following two stages:

$$^{8}\mathrm{Li} \rightarrow {}^{8}\mathrm{Be}^{*} + \beta, \text{ and } {}^{8}\mathrm{Be}^{*} \rightarrow \alpha + \alpha$$

One typical example of alpha decay tracks from the 2+ excited state of ^{8}Be, was found in KISO event [7,8]. The two alpha tracks decay into back-to-back direction. The range of each alpha tracks can be seen around 5 μm in the nuclear emulsion. A lot of alpha decay tracks from ^{8}Be* in addition to the decays of thorium and uranium series can be found in the nuclear emulsion of E07 experiment. A sample of hammer track event is presented in Fig. 3.3.

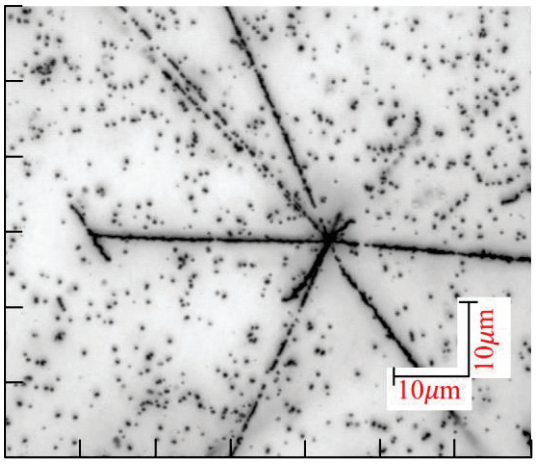

Fig. 3.3 Hammer track event found in the nuclear emulsion of E07 experiment.

3.5. Image scanning methods

In order to calibrate the density for the needs of Range-Energy relation in the emulsion, it is necessary to collect several tens alpha events. E07 experiment were aimed to detect 100 double-Λ hypernuclei. To analyze these expected hypernuclei, several thousand alpha decay events are needed to detect in a reasonable time. In the previous time, alpha decay search with human eyes took half to one hour for one event. The conventional method was time consuming to get enough alpha number. Therefore, "Overall scanning method": "Vertex picker", and "CNN-based event classifier" has

been developed to search alpha decay event with timeless scanning by Yoshida et.al [22, 23].

3.5.1. Overall scanning method

This is a way of searching the events in the emulsion layers using a computer-controlled microscope. The magnification of the objective lens is 20x which has 1140μm x 200μm field of view (FOV) and the numerical aperture is 0.35. A high-speed, high-resolution camera captures images of the tracks beneath the microscope. To take photos and select out vertex-like forms, a specific image processing approach is used, which consists of numerous "black tracks". The image processing settings are optimized using E373 experiment emulsion sheets to identify alpha decay vertices with a reasonable Signal-to-Noise ratio.

The first phase is grain enhancement and binary thresholding, as seen in Fig. 3.4. The "difference of Gaussians" method is used. The original image is transformed into a blurred image using a Gaussian kernel. A difference-image can be created by subtracting the blurred picture from the original image. By employing a threshold brightness value to distinguish black and white pixels, all of the pixels in the difference image are turned into binary brightness information. The threshold has been chosen to be approximately 25% of the maximum brightness image. The number of pixels over the threshold per view is $26 \pm 6 \times 10^3$. In a shrunk emulsion layer, it is equivalent to 20 pixels per square and 10 μm on each side.

The second phase is noise reducing and thinning. There are $6 \pm 1 \times 10^3$ blobs in a binarized image, which are the groups of pixels with high brightness after "difference of Gaussians." In a shrunk emulsion layer, it is equivalent to 4.2 ± 0.6 blobs per square, 10 μm on each side. Thresholding is used for screening bold tracks, such as alpha tracks, with a condition of the contour length and size of a blob being less than 5 and 10 pixels, respectively. Small blobs like noises are removed by this thresholding, whereas nearly hundred blobs are survived. With the use of a thinning algorithm at the end of this stage, the tracks become thin lines with a width of one pixel.

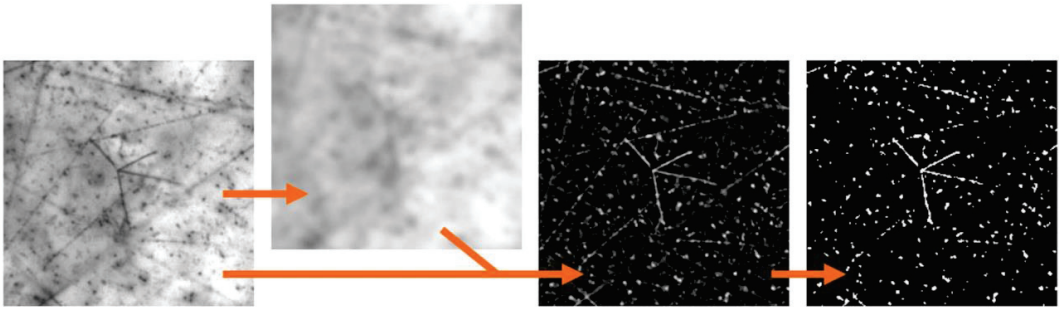

Fig. 3.4 The first step of the image processing for vertex detection, i.e., raw image, Gaussian-blur, difference of Gaussians and binary thresholding from left to right. The area of the FOV is 120 × 120 μm^2, which are cropped from the original FOV having 1140 × 200 μm^2. The image was taken from ref. [22].

The detection of line segments and vertices is the third phase. Line segments in an image are recognized and grouped using the "Probabilistic Hough transformation" technique if an edge point of one line segment is near to that of another. This stage will choose vertex-like forms with many lines. Duplicated vertices that share line segments are combined. If the area of the convex hull, which is the smallest polygon containing the line segments, is greater than a threshold area, an item is determined to be a vertex-like form. Fig. 3.5 represents the second and third steps.

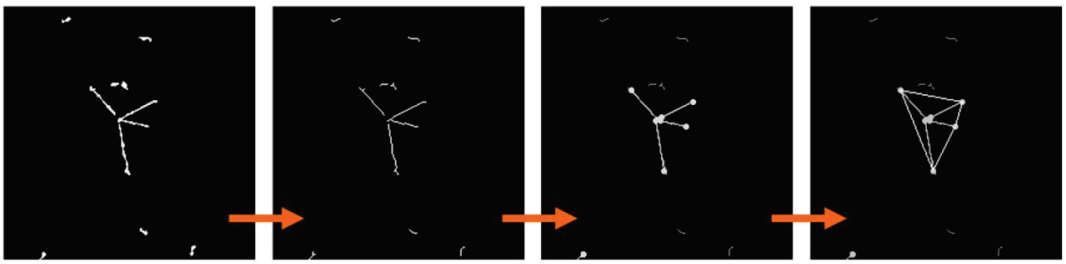

Fig. 3.5 The second and third step of the image processing: noise reduction, thinning, line detection and vertex detection. The image was taken from ref. [22].

3.5.1.1. Imaging to remove non-vertex events with a 50x lens

To minimize non-vertex images, we retake cross-sectional micrographs with a 50x lens for each object found by the primary selection. Almost 60% of the items picked by primary selection were not vertex, indicating misrecognition of cross tracks. Because the resolution and contrast of the secondary pictures are better than those of the primary

ones, they are efficient for distinguishing between cross tracks and vertices. The 50x lens has a FOV of 130 110 μm^2 with a resolution of 0.26 μm per pixel. Fig. 3.6 depicts a schematic representation of this two-stage picture capture process.

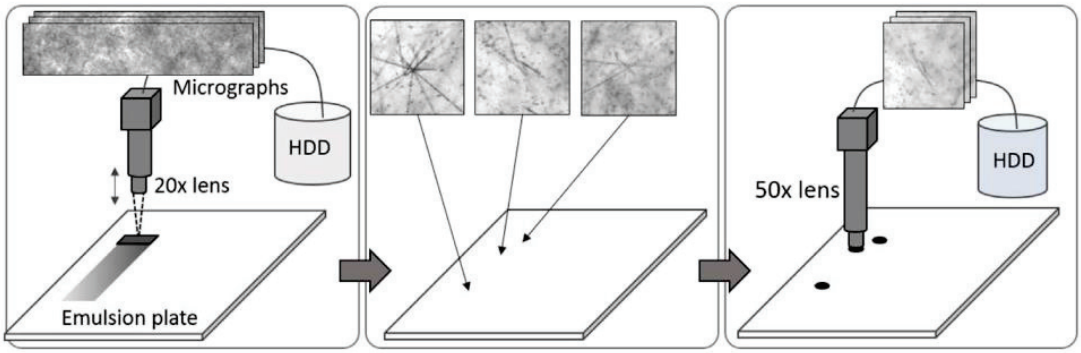

Fig. 3.6 The two-stage image taking. Cross-sectional micrographs are retaken by a 50x lens for each object detected by a 20x lens as the primary selection. The image was taken from ref. [22].

For the retaken micrographs, secondary image processing is used. This procedure is similar to the primary one, but some of the parameters, such as magnification, are tuned based on the optical circumstances. The focal depth of the 50x lens is narrower than that of the 20x lens, corresponding to 6 μm emulsion layer thickness. To achieve an adequate focus depth, numerous cross-sectional micrographs are projected onto a superimposed picture at the start of secondary image processing.

The final step is to perform a visual check to determine if the retrieved objects are alpha decay events. We divide the objects into many groups, and an alpha decay can be observed if the item has four or five black tracks with lengths of roughly 30 μm. After applying this method, 212 alphas decay events were detected in 7.7 hours of eye check. This method is nearly 20 times more efficient than that of conventional method.

3.5.2. CNN based event classification

The schemes introduced above for J-PARC E07 adopted an overall scanning approach called Vertex Picker. This technique finds vertex-like features with three or more tracks starting from a single location in comprehensive micrographs of thick emulsion sheets. The system generates cropped images of the vertex candidates and

information about their track after using image processing techniques. However, this method also selects numerous other vertex-like items, such as an alpha-decay event and a beam-nucleus interaction, as well as non-vertex objects, such as a cross of unconnected tracks and a dark patch that resembles dust. Therefore, the ratio of the interesting vertex events and the other events that were observed is unsatisfactory.

As a remedy to the above shortcomings, a new approach for detecting vertex-like objects is proposed applying a convolutional neural network (CNN). The objective in this case is to detects candidates of vertices, that are related to double hypernuclei efficiently. To achieve this, sufficient amount of training and validation data is required.

3.5.2.1. Data preparation and architecture of CNN model

Vertex Picker was used to choose alpha-decay events for the building of an event classifier for categorizing alpha-decay events using a CNN. A total of 112 958 images from six 50 mm 50 mm 0.5 mm similar volumes of two emulsion sheets from the J-PARC E07 experiment was selected. A total of 1120 photos of alpha-decay events and 18793 photographs of non-alpha-decay events were selected through visual assessment. The photos were randomly dispersed in the training (TRAIN) and validation (VALID) datasets in a 4:1 ratio.

The proposed CNN architecture is shown in Fig 3.7. Conv1, the first convolution layer, is a convolution layer with 64 output channels and a stride of two pixels that is 7 pixels x 7 pixels. The next layer is a maximum pooling layer of 3 pixels by 3 pixels with a stride of two pixels. Convolutions are also performed by the following layers, which range from conv2 to conv5. Following these layers is a global average pooling layer. The CNN's final component, the fully connected layer, is implemented in three phases to produce a scalar value. The discriminant function's threshold, which is used to discriminate between positive and negative samples, is typically 0; however, the threshold can be modified based on the desired purity and detection efficiency of a selection.

In this technique, oversampling method [24,25] and RandAugment concept [26,27] was employed. By defining two hyperparameters, N and M, RandAugment automatically and randomly conducts several image transformations. N represent the

number of image transformations and M is the magnitude of the image transformations within the range of 0-30.

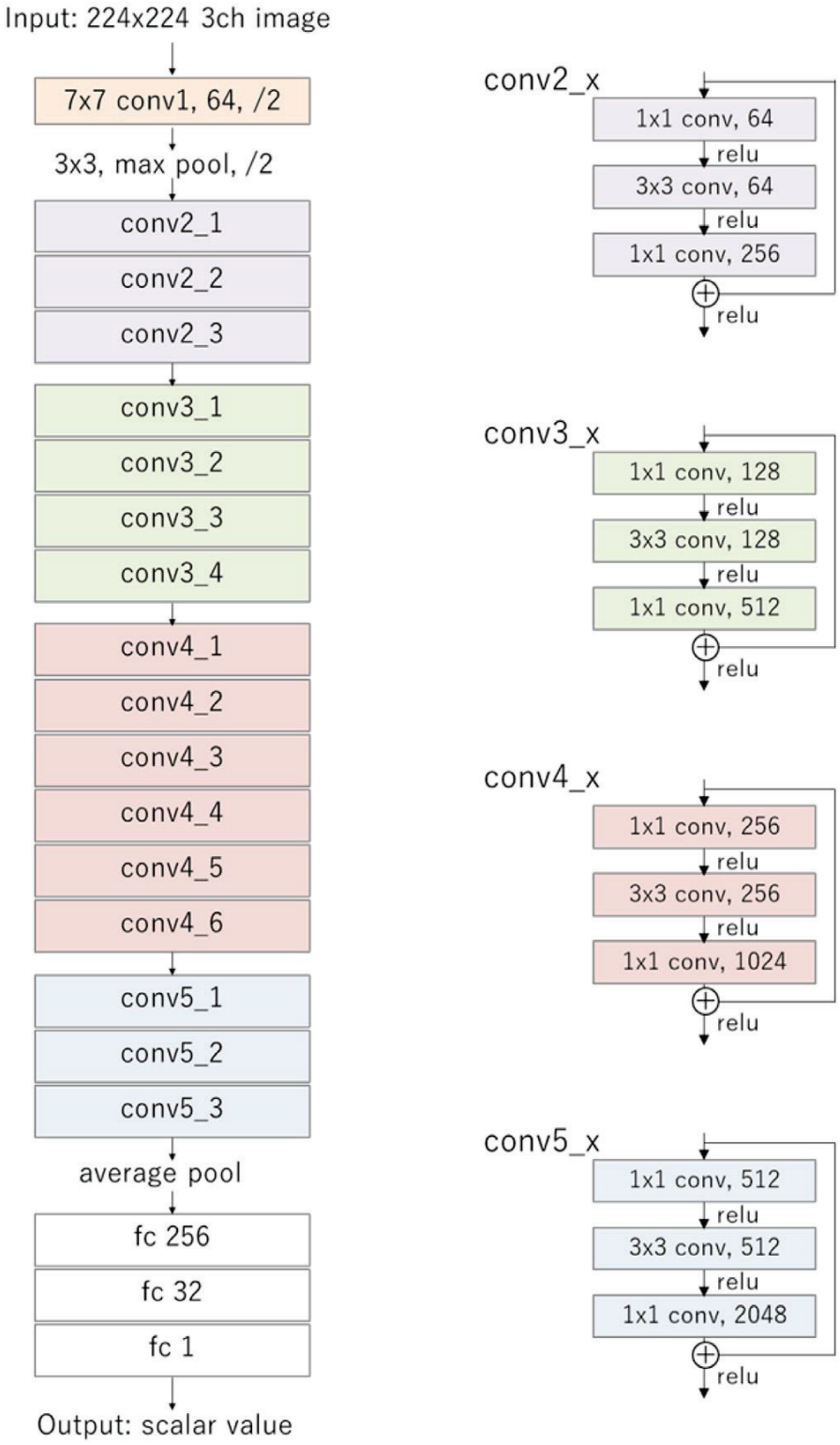

Fig. 3.7 A flow chart of the CNN architecture based on ResNet50. The total number of weight parameters of this CNN was 24 million. The figure is taken from ref. [23].

For optimization, the model Adam optimizer was applied with binary cross entropy loss function [28]. Further, transfer learning was necessary since the number of images used in the development was insufficient to train the CNN from a random state. In this case, the ResNet50 model was used as backbone.

3.5.2.2. Trained CNN model and performance

To evaluate the performance of the classifiers, the area under the precision–recall curve was used as the performance metric [29]. The curve is made up of pairs of two parameters, commonly known as precision and recall, that are used at various threshold values to distinguish between positive and negative samples based on CNN output values. Here, recall reflects the effectiveness of the classifier's selection process while precision relates to the purity of the classified samples. The Fig. 3.8 gives the different models and precision derived from iterative process. The best combination was achieved with (N = 4, M = 30), and the best score obtained was 0.979 ± 0.002.

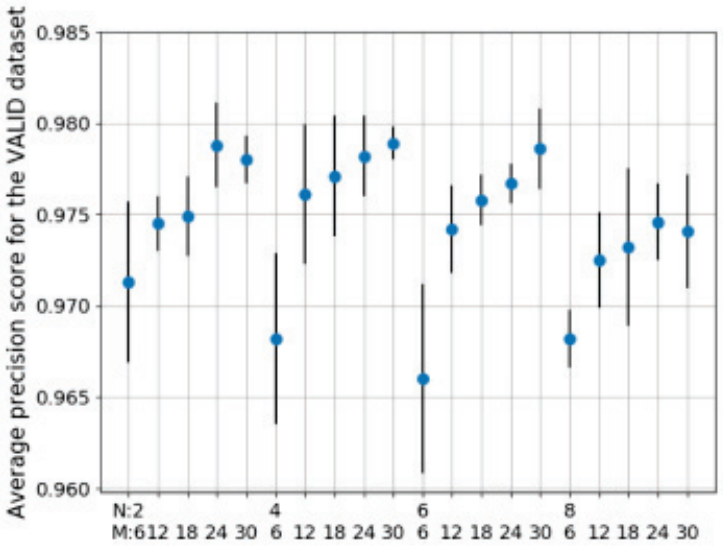

Fig. 3.8 Average precision score for the VALID dataset for various pairings (N, M) for RandAugment. The best value is 0.979 ± 0.002 at (N = 4, M = 30). The figure is taken from ref. [23].

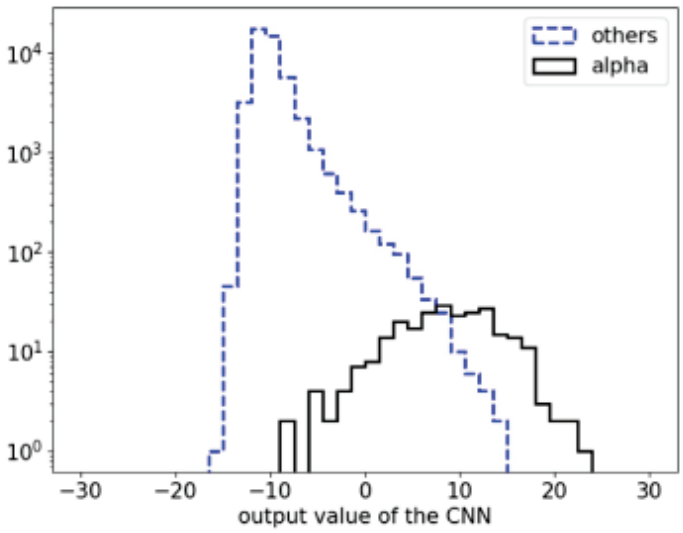

Fig. 3.9 Distribution of the output values of one of the best CNN models at (N = 4, M = 30) for alpha-decay and other events in the TEST dataset. The figure is taken from ref. [23].

Fig. 3.9 shows the test distribution of output values of CNN models (N = 4, M = 30) for the alpha-decay and the other events. It was observed that the values for the non-alpha-decay events were distributed mainly in the negative region, whereas the distribution of the output values for alpha-decays was shifted to positive values. The efficiency of CNN method was tested by comparing with the former method. The test results are shown in Table 3-1.

Table 3-1 Comparison of performances between former method (w/o CNN) and the developed CNN method (w/ CNN) at similar recall.

Method	Precision	Recall	Number of candidates
w/o CNN	0.081 ± 0.006	0.788 ± 0.056	2489
w/ CNN	0.571 ± 0.017	0.788	350 ± 10

From the above, the CNN method reduced the load of visual inspection by a factor of approximately 1/7, in comparison to the former method without a CNN.

3.6. Event selection with Classification Viewer and 50x objective lens

Several raw images were taken using developed methods: overall scanning and mask CNN. The output images are mixing with alpha, beam interaction, one-vertex, two-vertexes, sometime three-vertex, cross track, black dot trash. The images of two

vertex and three vertex candidates, and alpha decay candidates for Thorium and Uranium series are selected by human eye with the help computer software, “Classification Viewer”. The classified images are needed to confirm which have vertex or not by putting the emulsion plate under 50x objective lens microscope.

Before the time of beam exposure, emulsion stacks were being stored in KAMIOKA mine more than two years. As the nuclear emulsion is very sensitive to every charged particle, a lot of background tracks in the air are recorded in the nuclear emulsion along storing time. In order to erase background tracks, the refresh process was applied. The refresh process erases some parts of recorded alpha tracks and makes the gaps along the track (thin track). That kind of alpha tracks were not considered for the density calibration to avoid the uncertainty in the measurement. Sometime alpha particle may collide with other charged particles and then alpha track kinks and changes the direction. So that, the energy uncertainty may appear in the measurement. Alpha tracks with no gaps and no kink point (thick tack) were used to calibrate the density of emulsion layer. Classified alpha images are shown in Fig. 3.10 (a), (b), and (c).

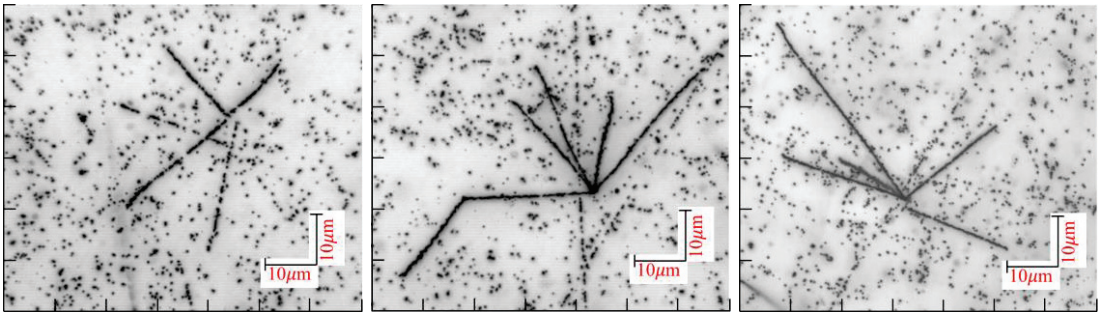

(a) (b) (c)

Fig. 3.10 Superimposed images of alpha decay events (a) with many gaps, (b) with kink track, and (c) with fine and black tracks found in E07 nuclear emulsion

3.7. Alpha range measurement with OverallViewer1

After checking the classified images with 50x objective lens, microscopic images were taken by 100x objective lens to measure accurately. The five hundred micrographic images were taken for each alpha event with 0.1 μm interval by changing an optic axis. Micrographic images can be combined as a set of images by image processing. Each image was processed with Gaussian blur to reduce noise image. As

an image enhancement algorithm, the brightness subtraction of the blurred image from original image was utilized to get good quality image. Alpha tracks can be constructed by using 500 cross-sectional images as shown in Fig. 3.11 (a) and (b).

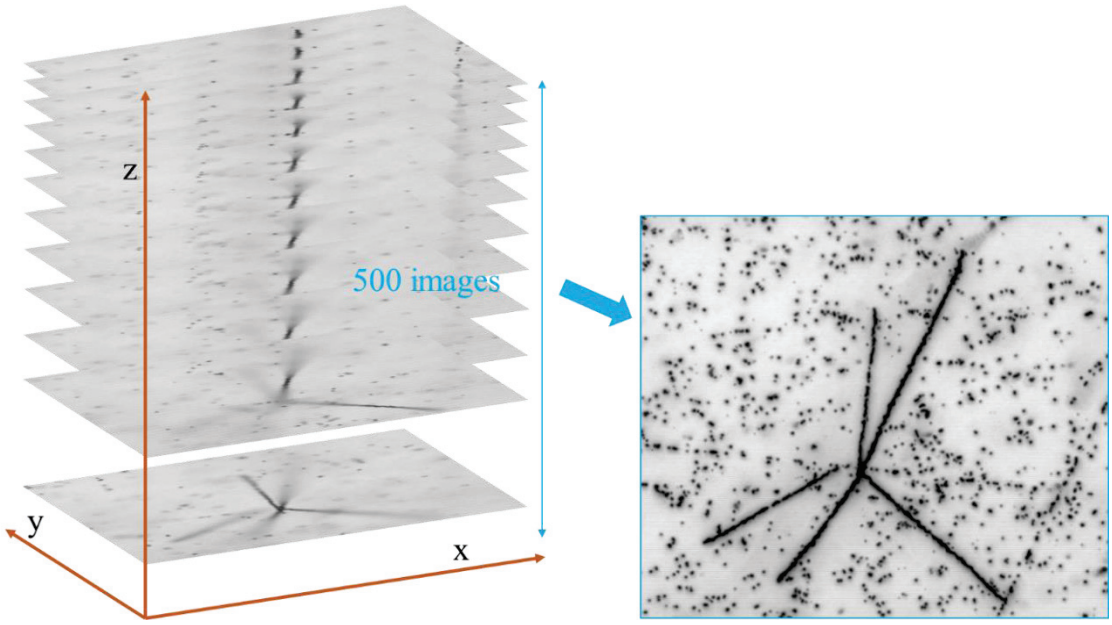

(a) (b)

Fig. 3.11 (a) A set of sequential images for one alpha with 0.1 μm interval and (b) Superimposed image with 500 cross-sectional images

For the alpha range calculation, x, y, and z coordinates of track position can be obtained from the processed image with the help of OverallViewer1. The track range can be measured accurately from the vertex point to the end point with the viewer. The track coordinates are taken by clicking several segments on the track range. The click position was decided by the brightness value. The pixel brightness value is zero inside of an alpha while the outside of an alpha has some brightness value. The x, y, and z coordinates are picked up from the most-darkest position.

3.8. Shrinkage factor, alpha track range and density calibration

For the calibration of density of emulsion layer, the alpha track generated by the decay of ^{212}Po in the thorium series, which had the longest track, and a monochromatic energy of 8.785 MeV was applied. The average range of alpha track was calculated

using the track's length in the three-dimensional Cartesian coordinates by the following equation:

$$R_{\alpha} = \sqrt{\Delta X^2 + \Delta Y^2 + (\Delta Z * S)^2} \quad (3.4)$$

where R_{α} is a range of alpha tracks; $\Delta X^2 = \sum_{i=1}^{n}(x_{i+1} - x_i)^2$; $\Delta Y^2 = \sum_{i=1}^{n}(y_{i+1} - y_i)^2$; $\Delta Z^2 = \sum_{i=1}^{n}(z_{i+1} - z_i)^2$; i is the i-th measurement point on a track; and S is the shrinkage factor in the z-direction, which is the same direction of the layer thickness and also the light axis of an optical microscope. To determine the value of S that gives an appropriate R of charged particles, ranges of the alpha track were initially calculated by varying S from 1.75 to 2.10 at intervals of 0.0025. Then, the appropriate S was adopted when the range distribution of alpha tracks for various angles has the minimum standard deviation (*Min_Stdev*) to provide an optimal mean range (*MR*). The error of mean range (MR_{err}) was calculated by multiplying the standard deviation (*Stdev*) of alpha track ranges with the inverse square root of the total number of alpha tracks. Fig. 3.12 (a) shows the standard deviation corresponding to S and (b) shows the distribution of the range using the determined value of S. Mostly, the range of that alpha tack can be seen around 50 μm in the nuclear emulsion. Then the density of emulsion layer can be calibrated by adjusting alpha track range and monochromatic energy of 8.785 MeV with the help of RE relation.

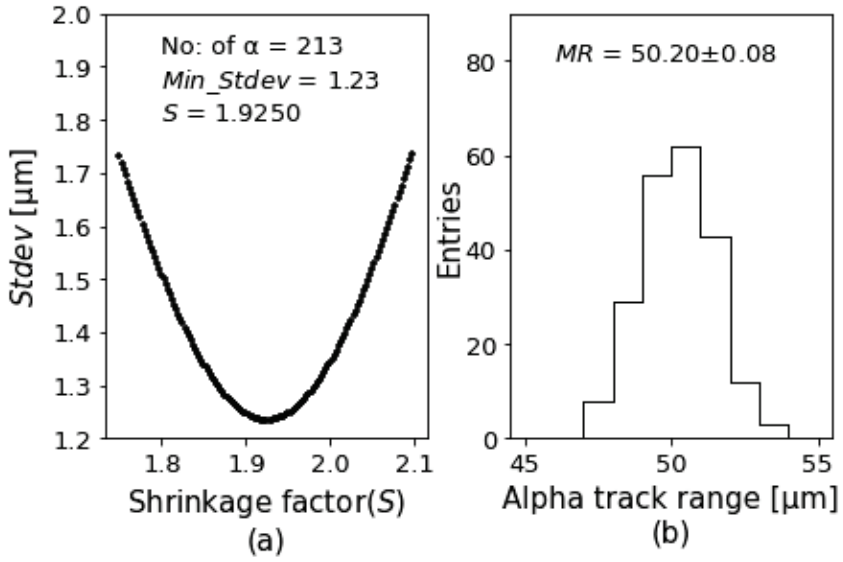

Fig. 3.12 Alpha range calibration. (a) The appropriate shrinkage factor *S* was extracted where the minimum standard deviation *Stdev* of range distribution. (b) Alpha track range distribution with the appropriate shrinkage factor.

CHAPTER 4

4. Estimation of Statistical and Systematic Errors

In this chapter, we will describe the detail of how to estimate the statistical [30] and systematic energy errors from the density of emulsion layer.

4.1. Statistical energy error from the density of emulsion layer

The range of a charged particles is the average distance traversed by a particle in the emulsion before its kinetic energy goes to zero. While computing the actual value of the range of charged particles in the emulsion, shrinkage factor due to photographic development and emulsion density must be considered. To get these factors, we have been used alpha particle from ^{212}Po of natural radioisotope. However, the relation between the number of alpha-decay events and the error of mass reconstruction has not been sufficiently studied. The sufficient number of alpha tracks is very important to obtain reasonable mass error of hypernuclei. In this section, we will express the detail of how to determine sufficient number of alpha tracks.

4.1.1. Alpha track range measurement

Firstly, alpha decay events were collected to determine a sufficient number of alpha decay tracks for the density calibration. With the developed scanning methods, around 500 alpha decay events were selected from three emulsion sheets, namely, PL #02, #03, and #04 from Module #030 of the E07 experiment. The shrinkage factor and mean range for each emulsion sheet were calibrated using the method express in section 3.8. The calibrated results are listed in Table 4-1. To confirm the consistency of the range distributions for three emulsion sheets, we applied the chi-square test for normal distributions. The range distributions for each emulsion sheet are shown in Fig. 4.1, Fig. 4.2, and Fig. 4.3. The calculated chi-square values of the alpha track range distribution for PL #02, #03, and #04 were 27.37, 21.27, and 26.29, respectively, with a degree of freedom (DOF) of 29. All the p-values for the three emulsion sheets are greater than the 0.05 level of significance as listed in Table 4-2. Therefore, the range distribution is sufficiently approximated by the normal distribution. This result indicates that the ranges of alpha tracks in the three emulsion sheets are consistent.

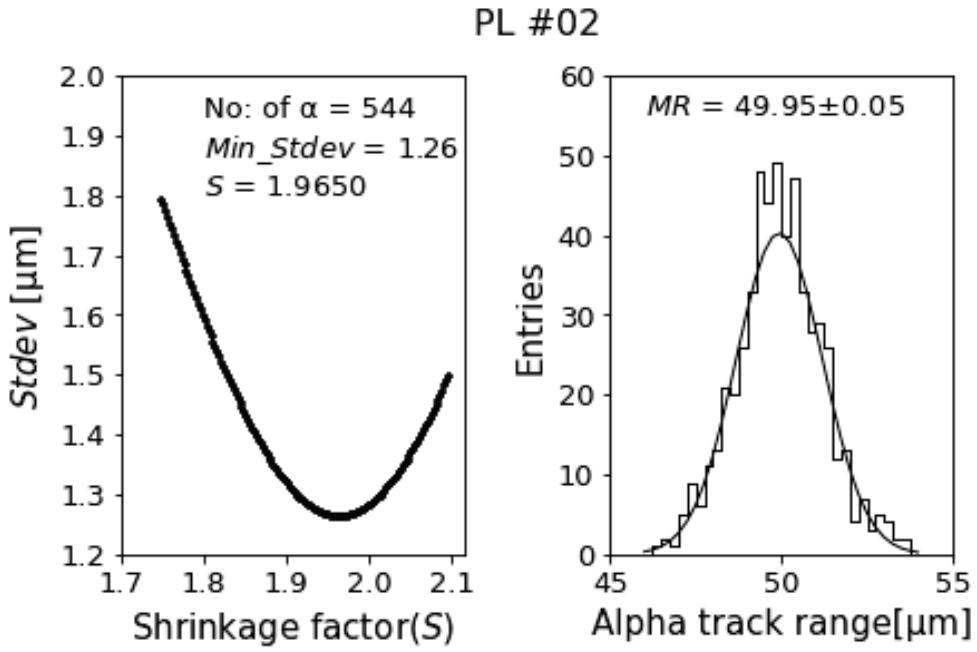

Fig. 4.1 Alpha range distributions for PL #02. All alpha tracks are in the range of 46–54 µm. The fitting distribution function represented with a solid line is Gaussian.

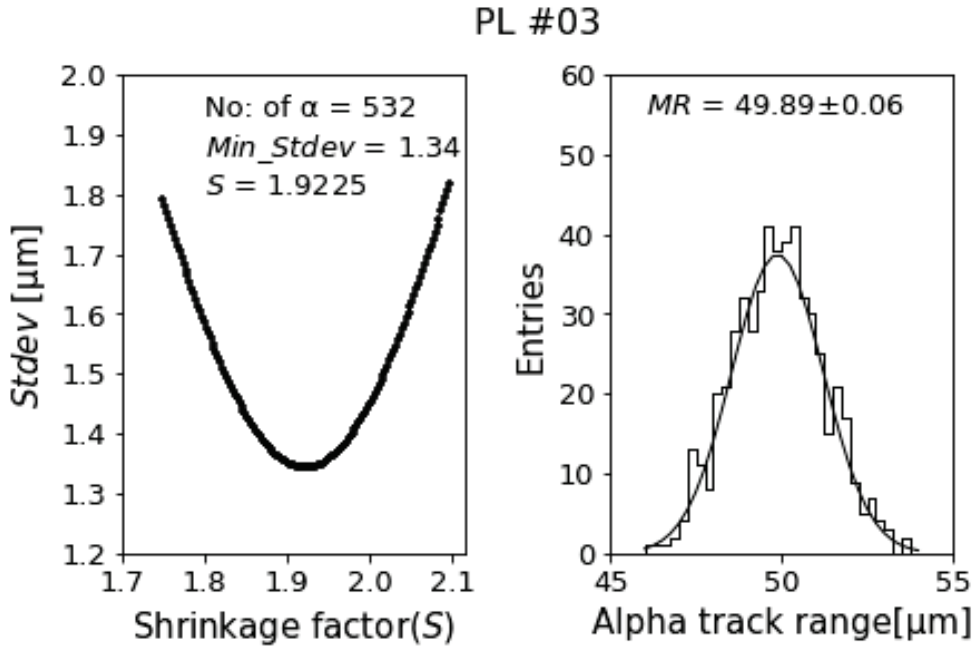

Fig. 4.2 Alpha range distributions for PL #03. All alpha tracks are in the range of 46–54 µm. The fitting distribution function represented with a solid line is Gaussian.

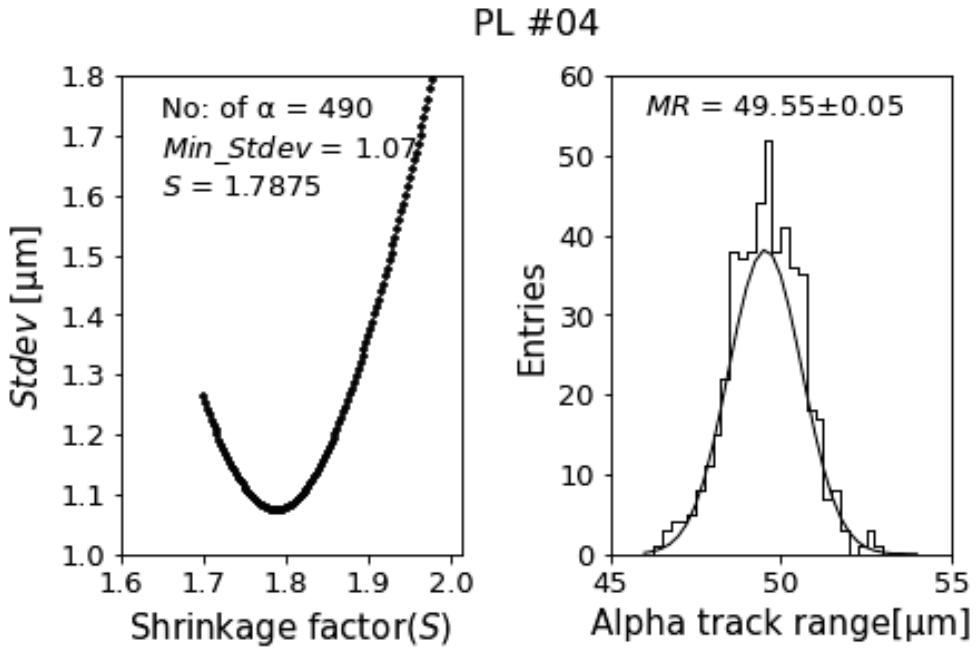

Fig. 4.3 Alpha range distributions for PL #04. All alpha tracks are in the range of 46–54 μm. The fitting distribution function represented with a solid line is Gaussian.

Table 4-1 Shrinkage factor and mean range for each emulsion sheet

Sheet number	Number of alpha tracks	Shrinkage factor	Mean Range [μm]
PL#02	544	1.9650	49.95 ± 0.05
PL#03	532	1.9225	49.89 ± 0.06
PL#04	490	1.7875	49.55 ± 0.05

Table 4-2 Chi-squared test values for the normal range distribution of each emulsion

Sheet number	Number of alpha tracks	Chi-square value	p-value
PL#02	544	27.37	0.552
PL#03	532	21.27	0.849
PL#04	490	26.29	0.610

4.1.2. Uniformity of the density of emulsion layer

Before determining the sufficient number of alpha tracks, the uniformity of density of emulsion layer in one emulsion sheet was checked by using alpha tracks from three different areas; near the center (A_C), left up corner (A_{LU}), and left down corner (A_{LD}) of PL #05 from Module #030 of the E07 experiment as shown in Fig. 4.4. The number of alpha tracks from areas A_C, A_{LU}, and A_{LD} were 213, 209, and 259, respectively. Range distributions for each area are shown in Fig. 4.5, Fig. 4.6, and 4.7.

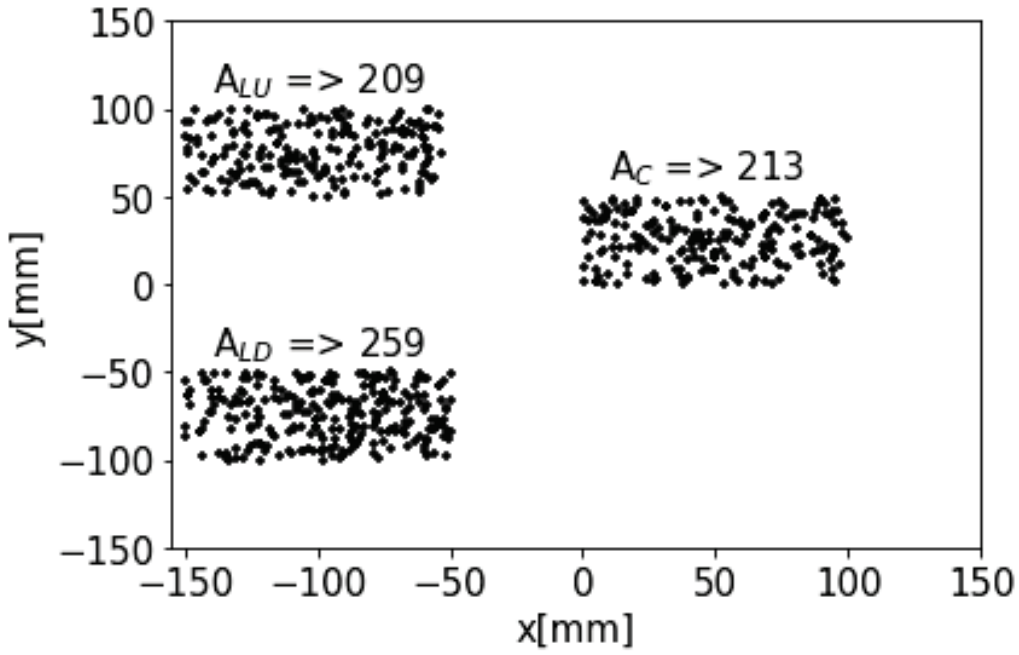

Fig. 4.4 Representing the alpha taken areas to check the density uniformity in one emulsion sheet.

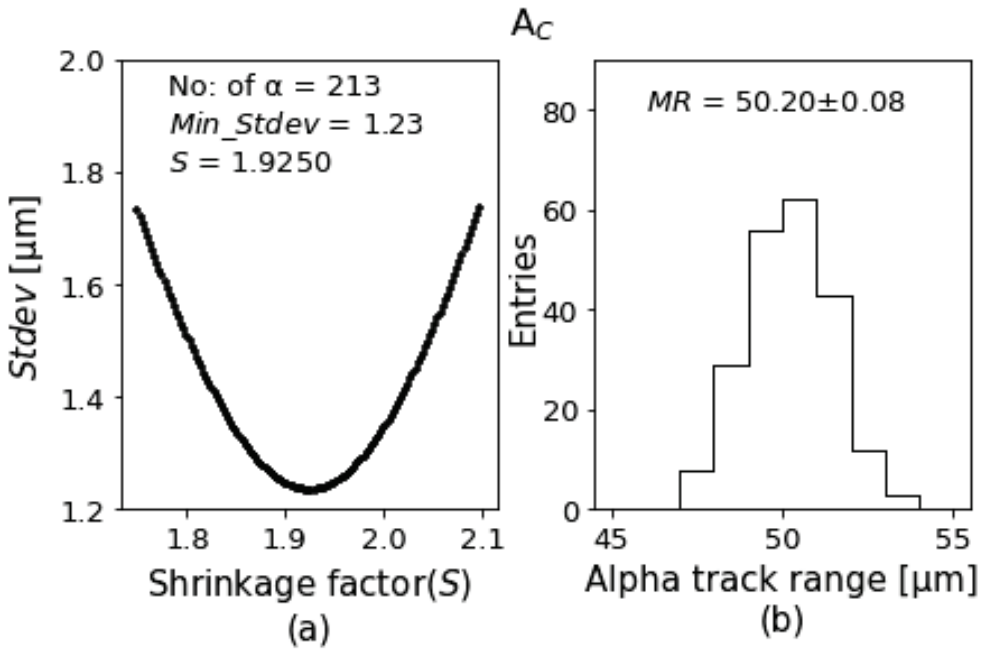

Fig. 4.5 Range distribution of the alpha tracks taken from near center (A_C).

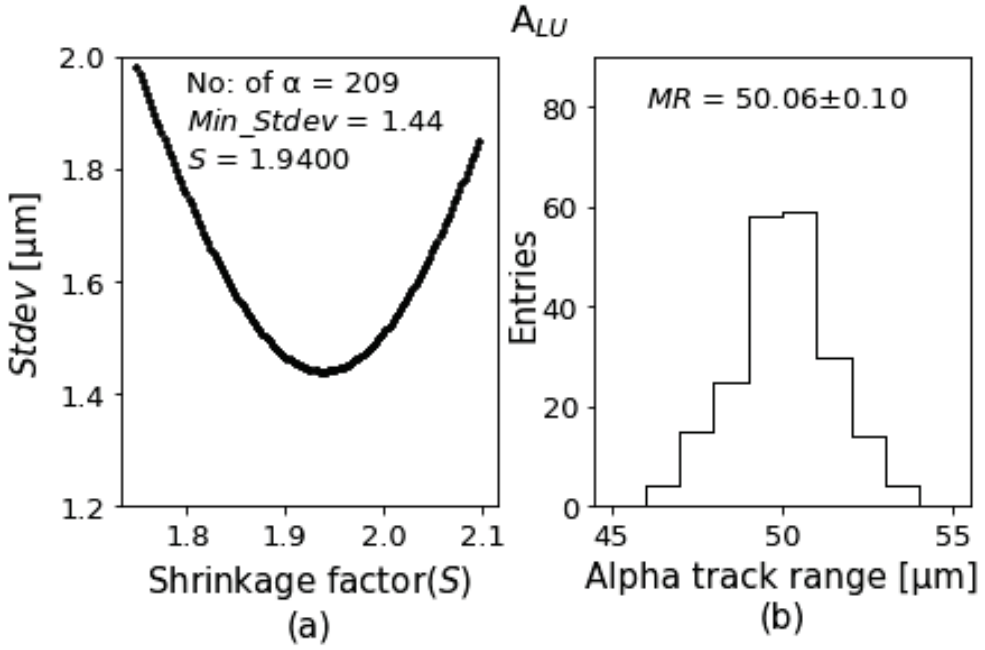

Fig. 4.6 Range distribution of the alpha tracks taken from left up corner (A_{LU}).

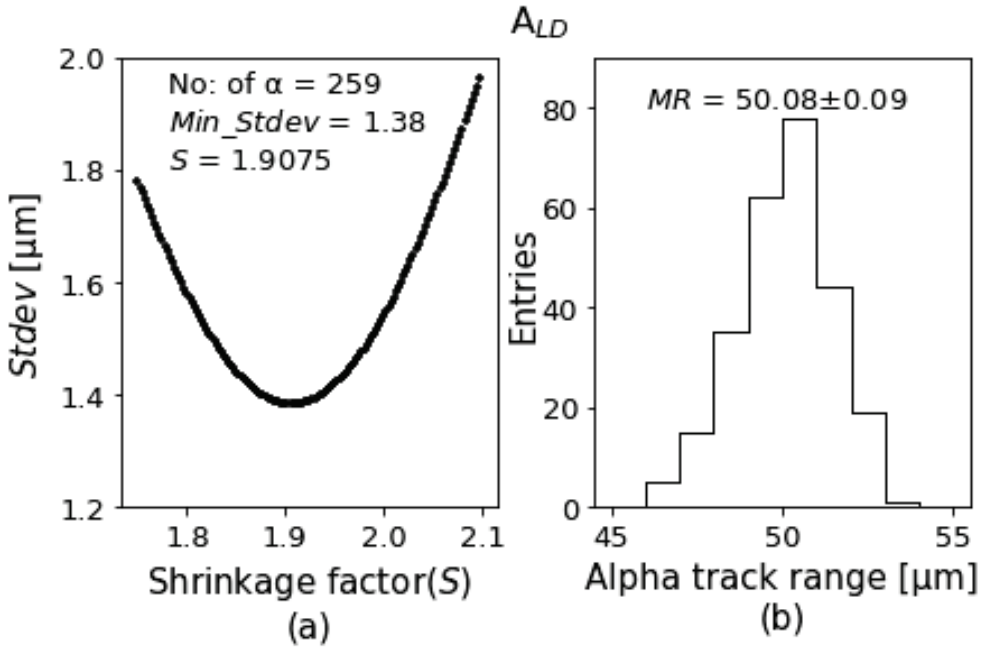

Fig. 4.7 Range distribution of the alpha tracks taken from left up corner (A_{LD}).

To check the density uniformity in one emulsion sheet, $MR \pm MR_{\mathrm{err}}$ were calculated by using 150 alpha tracks that are randomly selected from each area as listed in Table 4-3. Then the densities and density errors of emulsion layer for each area were calculated using $MR \pm MR_{\mathrm{err}}$. The results point out that the densities of emulsion layer in one emulsion sheet are uniform within 1σ of the measurement error.

Table 4-3 Calculated densities of emulsion layer from three areas labeled A_C, A_{LU}, and A_{LD} of PL #05 from the Module #030 of J-PARC E07 experiment.

Area [cm^2]	Number of alpha tracks	d [$g \cdot cm^{-3}$]	d_{err} [$g \cdot cm^{-3}$]
A_C (5cm*10cm)	150	3.558	0.012
A_{LU} (5cm*10cm)	150	3.565	0.013
A_{LD} (5cm*10cm)	150	3.562	0.013

4.1.3. Optimum count number of alpha tracks

To determine the sufficient number of alpha tracks, firstly, the ranges of alpha tracks were calculated using randomly selected number of alpha tracks from each emulsion sheet (PL #02, #03, and #04). These alpha tracks were categorized into six groups as 10, 50, 100, 150, 200, and 250 tracks (i.e., groups classified with total track number for each group, respectively). Then, densities and density errors of emulsion layer for each group are calculated with the obtained mean range of alpha tracks. As shown in Table 4-4, d for the six groups vary from 3.574 to 3.643 g·cm^{-3} and they are uniform within 3σ in three emulsion sheets. The average of d_{err} decreased with an increase in the count number from group 10 to 100, and it seemed to be saturated from group 150 to 250. Therefore, it may be sufficient to take at least 150 alpha tracks for calibration.

Table 4-4 The d and d_{err} for the groups with a different number of alpha tracks taken from three emulsion sheets. The unit is g·cm^{-3}.

Number of alpha tracks	Density (d) and Density error (d_{err})	PL #02	PL #03	PL #04	Average
10	d	3.617	3.574	3.613	3.601
	d_{err}	0.047	0.047	0.052	0.049
50	d	3.589	3.609	3.643	3.613
	d_{err}	0.022	0.022	0.018	0.020
100	d	3.596	3.589	3.624	3.603
	d_{err}	0.014	0.016	0.013	0.014
150	d	3.596	3.579	3.626	3.600
	d_{err}	0.011	0.012	0.010	0.011
200	d	3.575	3.604	3.619	3.600
	d_{err}	0.010	0.011	0.009	0.010
250	d	3.595	3.586	3.607	3.596
	d_{err}	0.009	0.009	0.008	0.009

4.1.4. Error calculation

Relationships between KE and KE_{err} of charged particles were analyzed and number of alpha tracks to be counted were examined from the calculated d and d_{err} values. Since the range distributions for three emulsion sheets were normally distributed and the obtained densities of emulsion layer were uniformed within 3σ, we took an approximate value (d_0) as 3.600 g·cm^{-3} for the KE and KE_{err} calculations. And the average of d_{err} (d_{err_avg}) was taken from the same number of groups for each emulsion sheet.

The range of proton was calculated by setting d_0 for the region where KE values were varied from 0 to 100 MeV at an interval of 10 MeV. Then, KE_{err} for three charged particles (proton, alpha (^{4}He), and lithium (^{7}Li)) were calculated using obtained range, d_0, and d_{err_avg} of each group in order to determine KE_{err} from the density error. Relationships between KE and KE_{err} of proton for each group are shown in Fig. 4.8. The gaps of KE_{err} in the groups 10, 50, 100, and 150 to the group of 150, 200, and 250 are large. As shown in Fig. 4.9, tendencies of KE_{err} gap for ^{4}He and ^{7}Li are similar to those for the proton, although there were small differences in KE_{err} among the referred particles. According to these results, we decided that utilizing at least 150 alpha tracks for the calibration was sufficient.

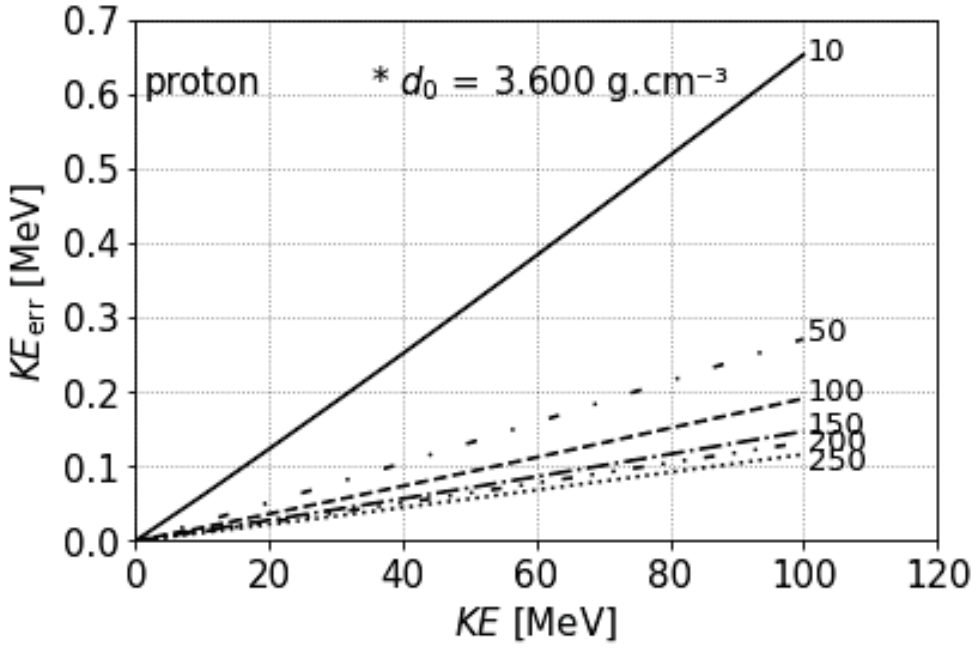

Fig. 4.8 Relationships between kinetic energy (KE) and kinetic energy error (KE_{err}) of the protons related to the number of alpha tracks

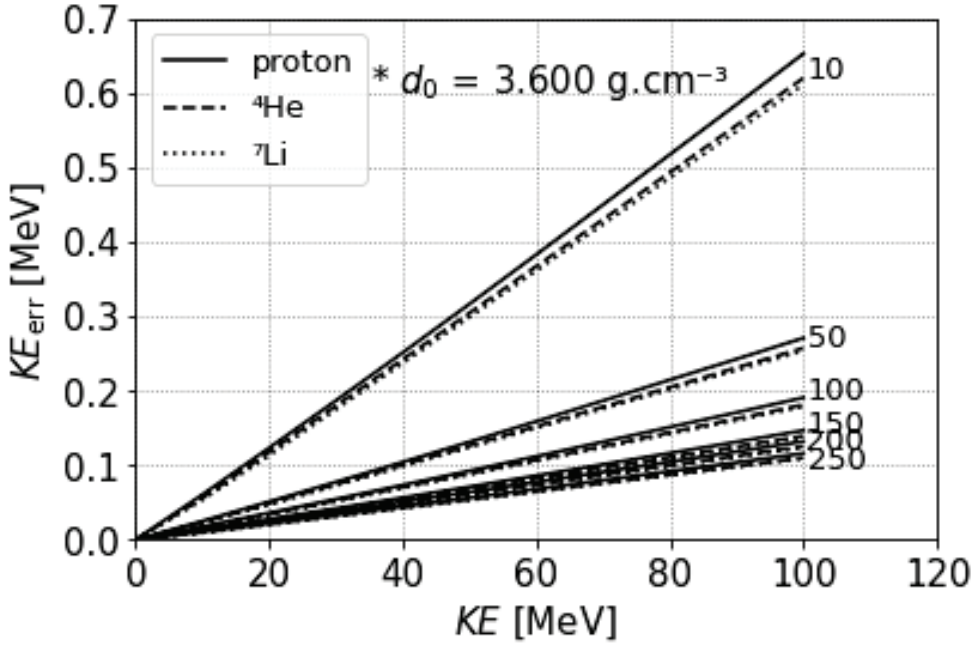

Fig. 4.9 Relationships between kinetic energy (KE) and kinetic energy error (KE_{err}) for three kinds of particles; proton, ^{4}He, and ^{7}Li related to the number of alpha tracks. The tendency of KE_{err} for ^{4}He, and ^{7}Li are similar to proton.

Although Table 4-4 indicates that the densities of emulsion layer varied from 3.574 to 3.643 g·cm^{-3}, we set d_0 as 3.600 g·cm^{-3} for the calibration. Therefore, we calculated the KE_{err} variation by changing d_0 with ± 0.1 g·cm^{-3}, where the density error of emulsion layer was set to be d_{err_avg}. As a result, the maximum ratio of the difference to KE_{err} was ± 2.35% (0.004 MeV) for the proton of 100 MeV. The heavier particles have smaller ratios than that of proton. The deviation generated by changing d_0 with ± 0.1 g·cm^{-3} was sufficiently small.

As ΔR is a statistical error in the analysis of double hypernuclei, the KE_{err} obtained from ΔR was also calculated. To compare the KE_{err} values obtained from the density error of emulsion layer and ΔR, KE was varied from 0.5 to 100 MeV at intervals of 0.25 MeV. We used d_{err_avg} of G-150 for the calculation of KE_{err}. As shown in Fig. 4.10, the KE_{err} from ΔR is one order of magnitude larger than that from d_{err_avg} for five particles, namely, the proton, ^{4}He, ^{7}Li, ^{9}Be, and ^{11}B.

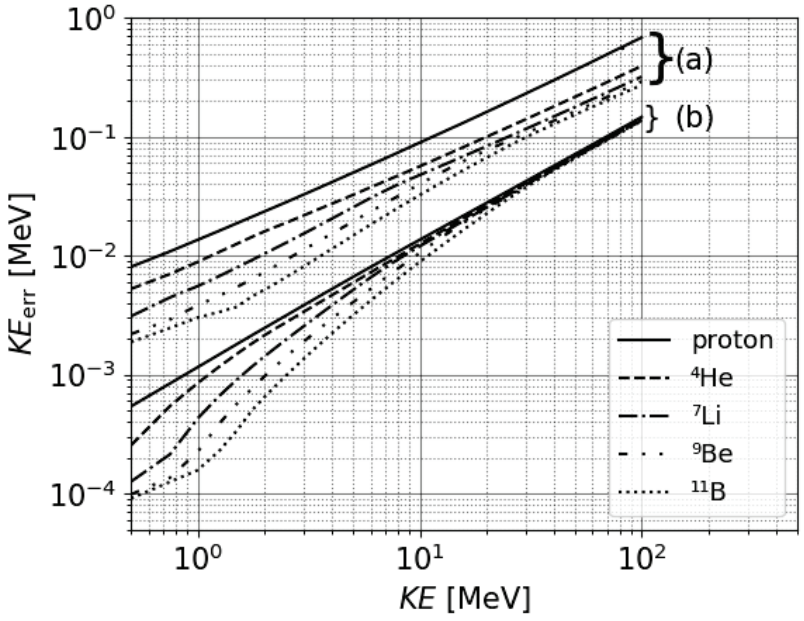

Fig. 4.10 Comparison of KE_{err} value for each KE obtained from (a) ΔR and (b) d_{err_avg} for proton, ^{4}He, ^{7}Li, ^{9}Be, and ^{11}B. This figure was taken from ref. [30].

4.2. Systematic energy error from the density of emulsion layer

Most of hypernuclei decay within a short range with low energy. In the analysis scheme of hypernuclei from E07 experiment, only the alpha decay tracks from ^{212}Po of thorium series which have monochromatic energy of 8.785 MeV are used to calibrate the density of emulsion layer. Hypernuclei may decay with a lower or higher energy than 8.785 MeV. If we draw RE relation curve for alpha particle ($^4_2$He) using the density calculated from the alpha decay tracks from ^{212}Po, the particles which possess charged (+2) should be line in RE relation curve. Fig. 4.11 show the RE relation curve for $^4_2$He. However, we have never checked for other energy regions. Therefore, since we have alpha decay tracks which possess different energies, we will investigate the uncertainties of RE relation. How much systematic energy error will be obtained in other energy regions?

In this section, we will investigate systematic energy error using alpha decay tracks from ^{212}Po (α_1), ^{214}Po (α_2), ^{226}Ra (α_3), and 2+ excited stated of ^{8}Be* (α_4) .

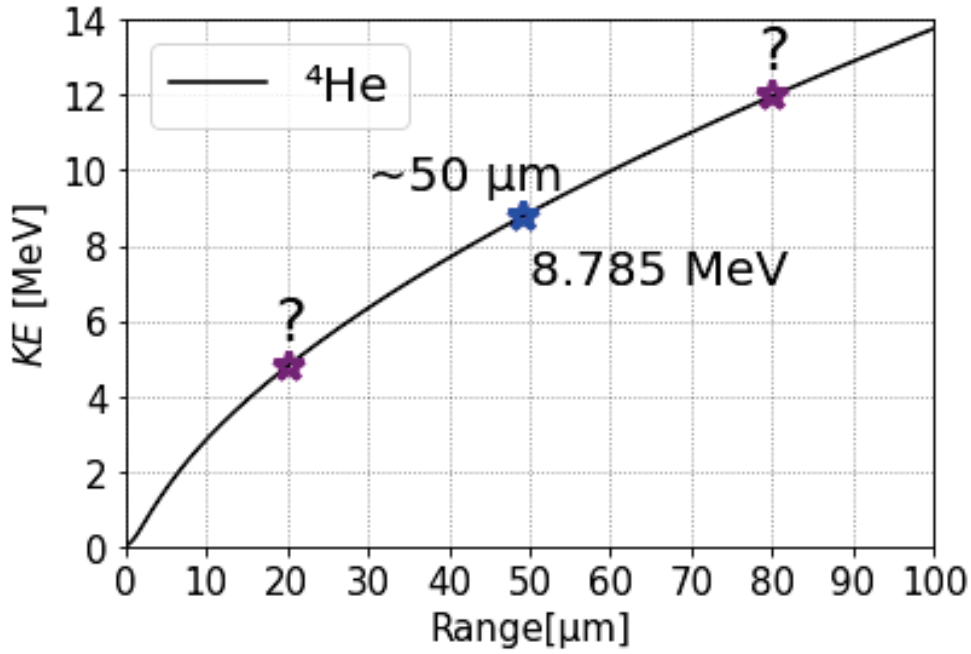

Fig. 4.11 The RE relation curve for ^{4}He using the calculated density from the alpha decay tracks of ^{212}Po

4.2.1. Range measurement for different kind of alpha tracks

To investigate systematic energy error, alpha decay tracks from PL #10 from Module #047 of the E07 emulsion experiment, were used. In section 4.1.4, the number of sufficient alpha decay tracks to minimize mass error of double hypernucleus was determined to be at least 150 for the density calibration. Therefore, at least 150 alpha decay tracks from ^{212}Po (α_1), ^{214}Po (α_2), ^{226}Ra (α_3), and 2+ excited stated of ^{8}Be* (α_4) were taken and will be used for the calibration. Currently, we have finished the analysis for α_1, α_2, and α_3. The analysis of alpha track from ^{8}Be*(2+), hammer track, is in progress.

For the first step, mean range of alpha decay tracks from ^{212}Po, ^{214}Po, and ^{226}Ra were measured. By applying the method expressed in section 3.8, shrinkage factor was calculated and determined to be 2.0075 with the minimum standard deviation of range distribution for alpha decay track from ^{212}Po as shown in Fig. 4.12. Using the adopted S, $MR \pm MR_{\mathrm{err}}$ for α_1, α_2, and α_3 were determined as listed in table 4-5. The range distributions for α_1, α_2, and α_3 are shown in Figures 4.13, 4.14, and 4.15, respectively.

Table 4-5 Measured ranges for each type of alpha tracks

Alpha decay type	Number of alpha tracks	Mean range [μm]
α_1	169	49.21 ± 0.09
α_2	176	40.12 ± 0.09
α_3	150	20.13 ± 0.08

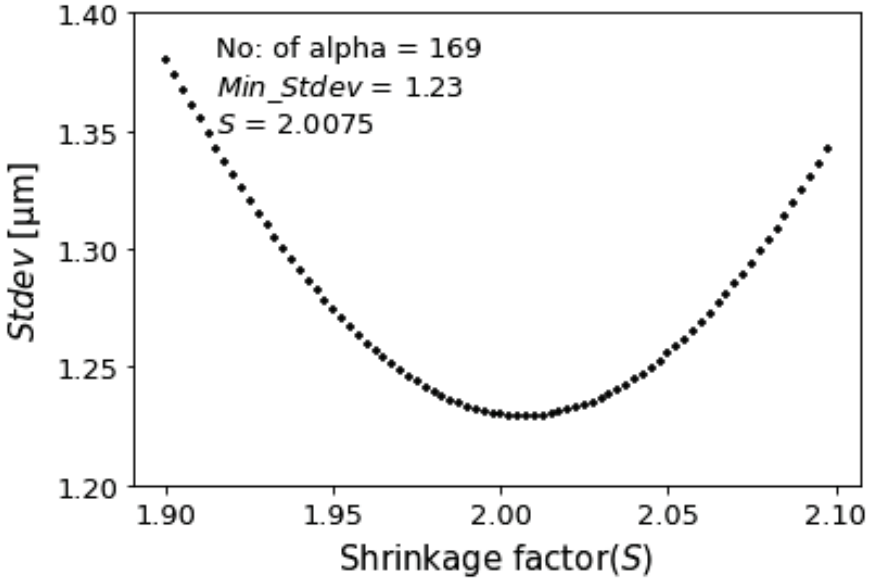

Fig. 4.12 Determination of shrinkage factor with minimum standard deviation of range distribution for alpha decay tracks from ^{212}Po

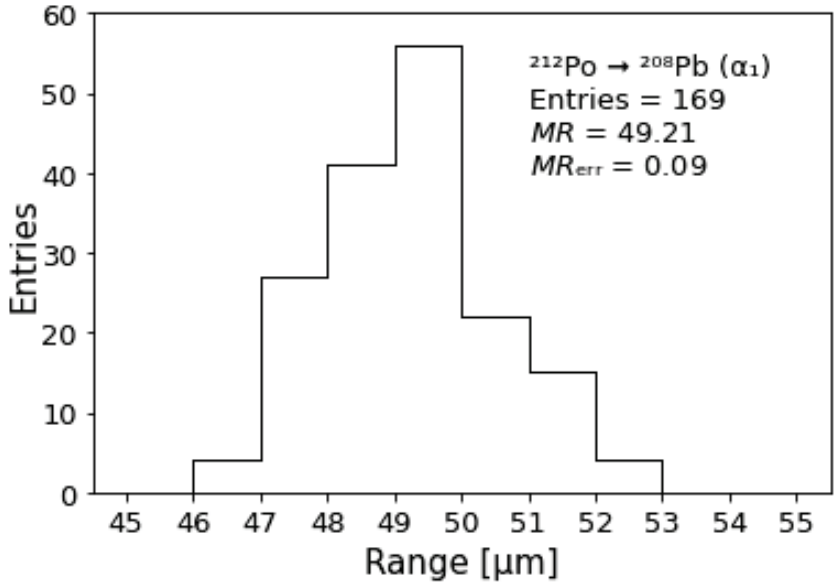

Fig. 4.13 Range distribution for the alpha decay tracks from ^{212}Po tracks which can be seen as longest tracks among other tracks.

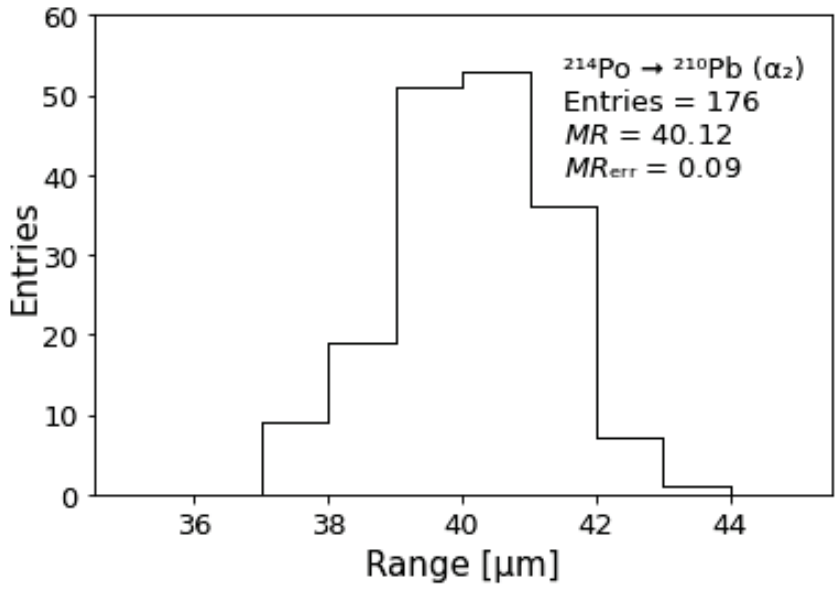

Fig. 4.14 Range distribution for the alpha decay tracks from ^{214}Po tracks which can be seen as longest tracks among other tracks.

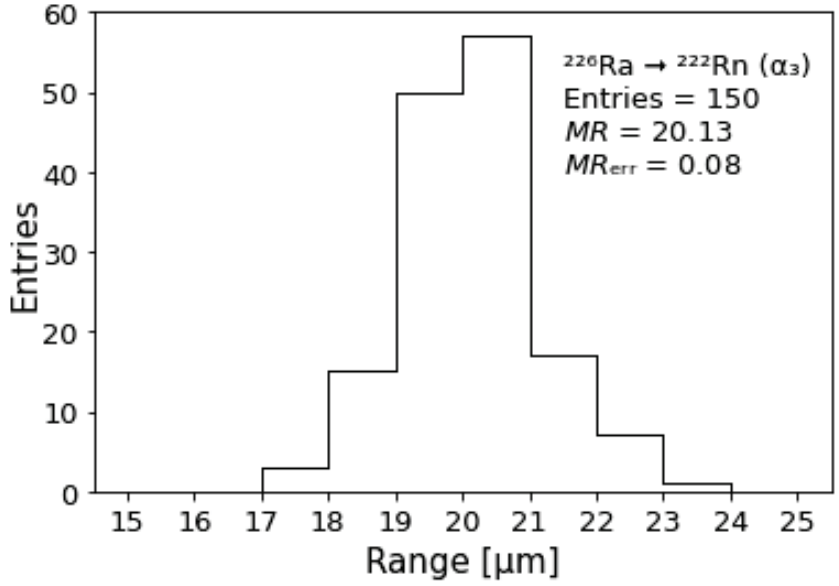

Fig. 4.15 Range distribution for the alpha decay tracks from ^{226}Ra which can be seen separately from other decay tracks.

4.2.2. Calibration of density of emulsion layer

Since we are investigating systematic energy error from the density of emulsion layer, as second step, the densities of emulsion layer are calibrated using calculated mean range and monochromatic energy of alpha decay tracks: α_1 (8.785 MeV), and α_2 (7.687 MeV). In the case of α_3, there are two possible energies such as 5.55 % of 4.602

MeV and 94.45 % of 4.784 MeV. Therefore, we will use the weight mean (4.774 MeV) of two values for α_3. The resulted densities are shown in Table 4-6.

Table 4-6 The calibrated density of emulsion layer for each kind of alpha decay track is listed in this table. The kinetic energy of α_1 and α_2 are monochromatic, but the energy of α_3 is taken into account the weighted mean value introduced in the text.

Alpha decay type	Kinetic energy [MeV]	Number of alpha tracks	Density [g·cm^{-3}]
α_1	8.785	169	3.664 ± 0.011
α_2	7.687	176	3.644 ± 0.013
α_3	4.774	150	3.615 ± 0.028

4.2.3. Estimation of systematic energy error

In connection to systematic energy error and the density of the emulsion layer, we will discuss uncertainties in RE relation with respect to the different densities. As shown in Table 4-5 and Table 4-6 from the previous sections, we have calibrated the mean ranges and densities of emulsion layer using α_1, α_2, and α_3. The kinetic energies (*KE*) of charged particles in the nuclear emulsion can be calibrated using known mass, charged, and range of charged particles, and the density of emulsion layer. Conversely, the range of charged particles can be calibrated using known mass, charged, and kinetic energies of charged particles, and the density of emulsion layer with the help of RE relation.

In this study, we want to know the systematic energy errors in different energy regions. Therefore, the graph of RE relation for $^4_2$He was created by varying the kinetic energy from 0.05 MeV to 10 MeV with an interval of 0.025 MeV. To know the systematic error form the density, the calibrated densities from α_1, α_2, and α_3, are used as an input values. The RE relation graph is shown in Fig. 4.16 (a). The RE relation curves for each energy region are shown in Figures 4.16 (b), and (c), respectively. The cross mark on the RE curve indicate the statistical errors obtained from the measurement. The statistical error of kinetic energy at each mean range of α_1, α_2, and α_3 are listed in Table 4-7. In the graph, the vertical axis represents the kinetic energy, and the horizontal axis represents the range of $^4_2$He .

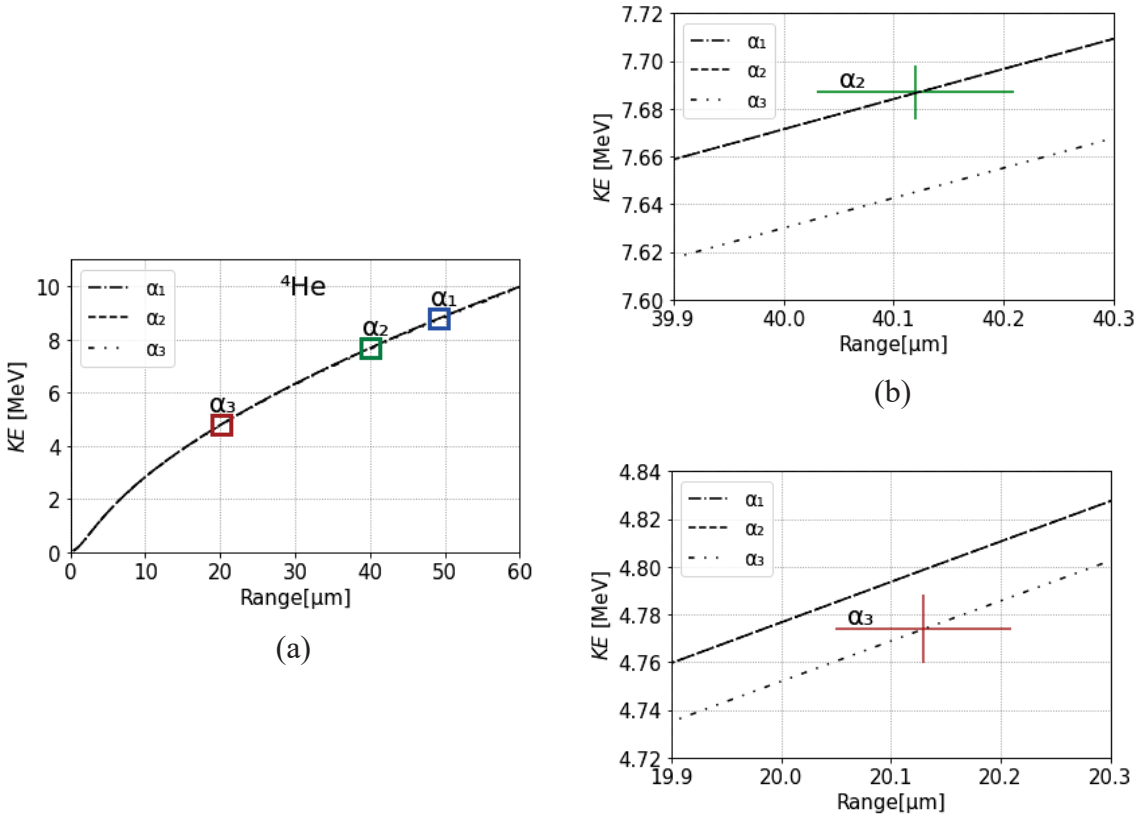

Fig. 4.16 (a) RE relation curve for ^{4}He particle using the densities of alpha decay tracks from ^{212}Po (α_1), ^{214}Po (α_2), ^{226}Ra (α_3). (b) The RE relation curve around 40.12 μm and 7.687 MeV. (c) The RE relation curve around 20.13 μm and 4.774 MeV.

Table 4-7 Mean range and kinetic energy with measurement errors

Mean range [μm]	Kinetic energy [MeV]
49.21 ± 0.09	8.785 ± 0.011
40.12 ± 0.09	7.687 ± 0.011
20.13 ± 0.08	4.774 ± 0.014

The range and kinetic energy with respect to the densities at each *KE* region are listed in Tables 4-8, and 4-9. The statistical are not expressed in the following Tables. Based on these results, we will discuss the systematic error of the kinetic energy for different energy region.

Table 4-8 The calculated kinetic energies at the range of 40.12 μm with different densities. The KE from α_1 and α_2 are identical because the density calibrated from them are the same.

Mean range [μm]	Density [g·cm^{-3}]	Kinetic energy [MeV]
40.12	3.664 (α_1)	7.687
	3.664 (α_2)	7.687

Table 4-9 The calculated kinetic energies at the range of 20.13 μm with different densities

Mean range [μm]	Density [g·cm^{-3}]	Kinetic energy [MeV]
20.13	3.664 (α_1)	4.798
	3.615 (α_3)	4.773

The systematic energy error is the deviation of kinetic energy by the different densities of emulsion layer. The systematic errors are categorized as follow.

1. The systematic errors due to the range of the alpha decay tracks from ^{212}Po and ^{214}Po at 40.12 μm is 0 keV as shown in Fig. 4.17. The error was calibrated by differencing the kinetic energies listed in Table 4-8.
2. The systematic errors due to the range of the alpha decay tracks from ^{212}Po and ^{228}Th at 20.13 μm is 25 keV as shown in Fig. 4.18. The error was calibrated by differencing the kinetic energies listed in Table 4-9.

The results show that the largest systematic energy error in RE relation which distributed from the different densities related to α_1, α_2, and α_3 is 25 keV (~4.5 MeV to ~9 MeV). Fig 4.19 shows the summary of systematic error for each *KE* region.

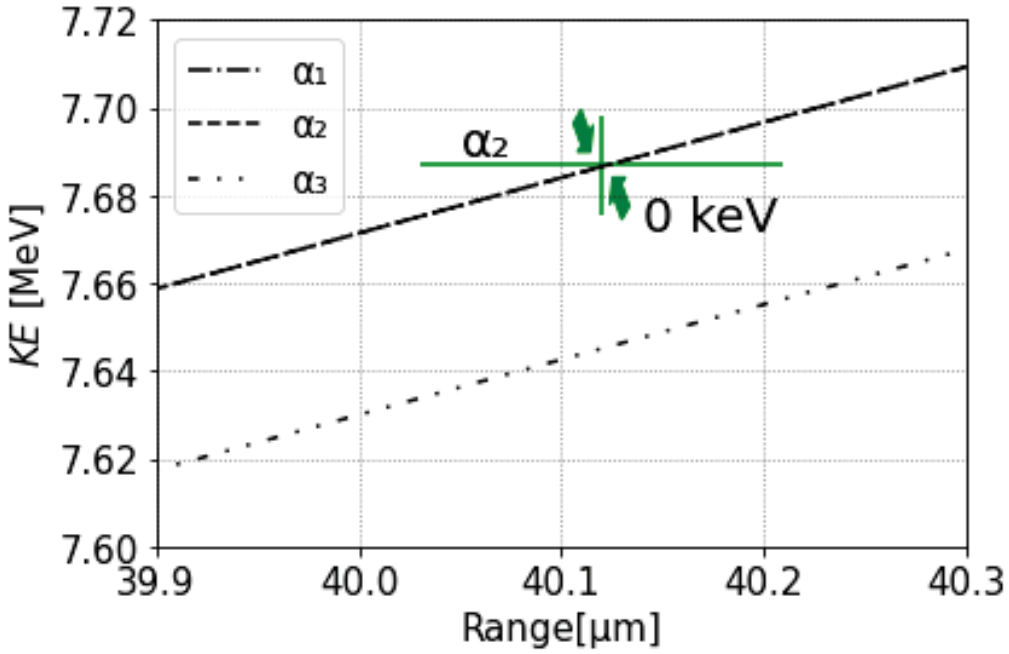

Fig. 4.17 Systematic energy error in RE relation at 7.687 MeV region (alpha decay track from ^{214}Po). The KE curve from α_1 and α_2 are identical because the density calibrated from them are the same.

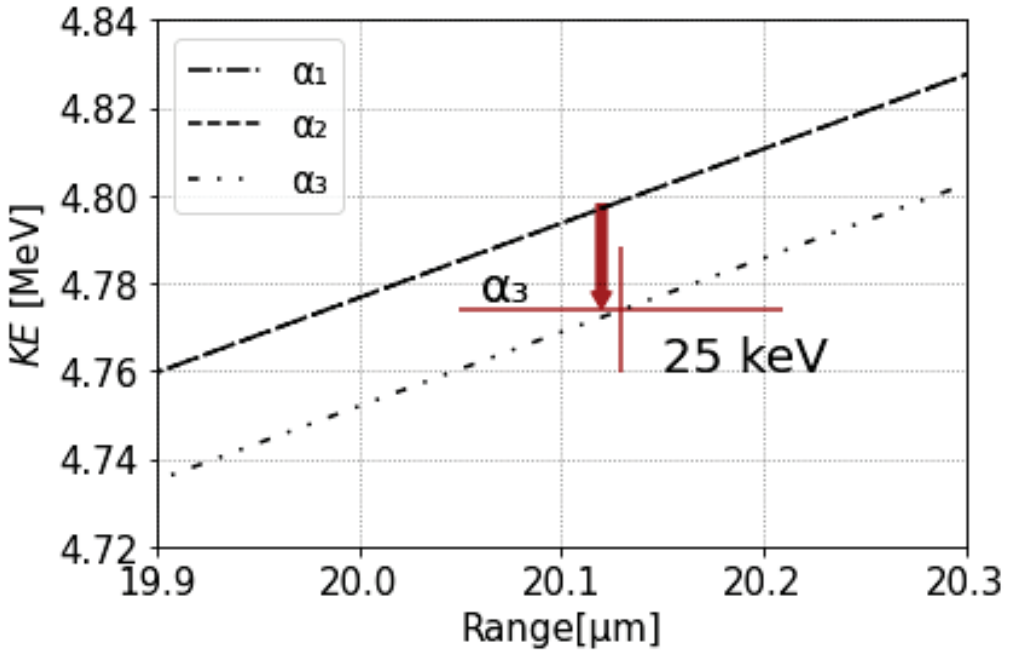

Fig. 4.18 Systematic energy error in RE relation at 4.774 MeV region (alpha decay track from ^{226}Ra)

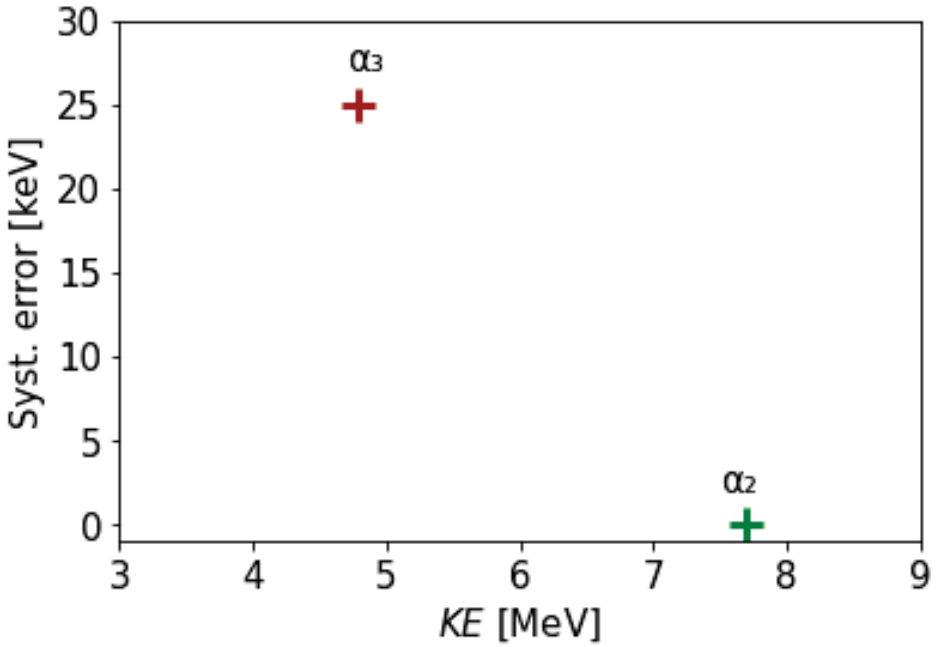

Fig. 4.19 Summary of systematic energy error which resulted from the density of emulsion layer for each energy region.

4.2.4. Application to the binding energy of IBUKI event

IBUKI event is a twin single-Λ hypernuclei which was found where the above alpha decay tracks are taken; in PL #10 of Module #47 from the J-PARC E07 experiment. The production and the decay modes were uniquely identified as follows.

$$\Xi^- + {}^{14}\mathrm{N} \rightarrow {}^{15}_{\Xi}\mathrm{C} \rightarrow {}^{10}_{\Lambda}\mathrm{Be} + {}^{5}_{\Lambda}\mathrm{He}$$

The binding energy of Ξ-*N* system (B_{Ξ^-}) was determined to be 1.27 ± 0.21 MeV [16]. B_{Ξ^-} error was determined from the measurement error (0.08 MeV) and the mass error of Ξ^-, ${}^{10}_{\Lambda}\mathrm{Be}$, and ${}^{5}_{\Lambda}\mathrm{He}$ (0.19 MeV). In this event, a daughter nucleus ${}^{5}_{\Lambda}\mathrm{He}$ possess charged (+2). The charged (+2) is same as the alpha decay track ${}^{4}_{2}\mathrm{He}$. The range of ${}^{5}_{\Lambda}\mathrm{He}$ is 87.7 ± 0.2 μm. Therefore, the range of ${}^{5}_{\Lambda}\mathrm{He}$ was used to extrapolate the systematic energy error in higher energy region than 8.785 MeV. However, ${}^{5}_{\Lambda}\mathrm{He}$ doesn't have monochromatic energy to calibrate emulsion density. We want to know the *KE* deviation by the emulsion density which calibrated from α_1 to others. Therefore, we will fit the density using α_2, and α_3 with their respective energies.

In this case, firstly, the kinetic energy at the range of α_2, and α_3 were calibrated by varying the density from 3.6 g·cm^{-3} to 3.7 g·cm^{-3} with an interval of 0.01 g·cm^{-3}.

Then, the errors are calibrated by differencing the originally defined *KE* and the calibrated *KE* at each point. The fitted density was decided by the minimum sum of *KE* error from α_2, and α_3 as shown in Fig. 4.20. It was determined to be 3.650 g·cm^{-3}.

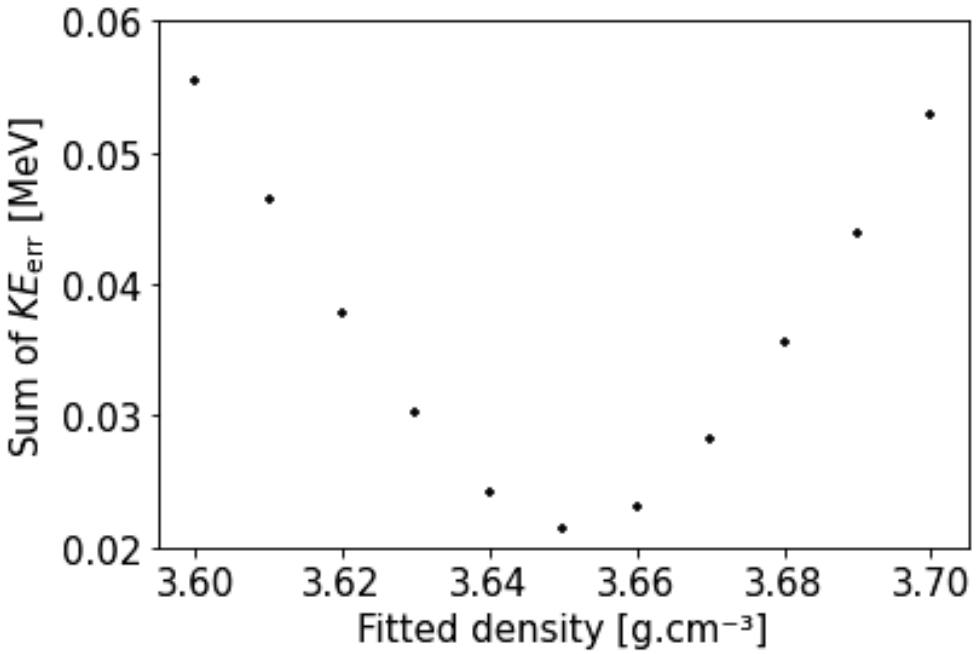

Fig. 4.20 The relation between fitted density and sum of *KE* error from α_2, and α_3.

Finally, the *KE* of ${}^{5}_{\Lambda}$He at 87.7 μm was calibrated using density from α_1 and the 3.650 g·cm^{-3} as shown in table 4-10. The result indicates that the systematic error at 87.7 μm is 22 keV. That is 1/10 of B_{Ξ^-} error of IBUKI event (0.21 MeV). When the systematic error from density of emulsion layer is added to the B_{Ξ^-} error of IBUKI event, the B_{Ξ^-} error is still 0.21 MeV. Therefore, the error taken in this event was reliable.

Table 4-10 The calculated kinetic energies at the range of 87.7 μm with three different densities

Mean range [μm]	Density [g·cm^{-3}]	Kinetic energy [MeV]
87.7	3.644 (α_1)	13.977
	3.650 (fit)	13.955

CHAPTER 5

5. Summary

The nuclear emulsion detectors have been used to investigate the interaction between *B*-*B* interaction; especially, Ξ-*N* and Λ-Λ interactions. From the emulsion experiments, the characteristics of significant double hypernuclear events have been clearly understood such as NAGARA and KISO events from KEK-PS E-373 experiment, and MINO event, IRRAWADDY event, IBUKI event, etc. from the J-PARC E07 experiment.

To understand Λ-Λ and Ξ-*N* interactions, binding energy of double hypernucleus is very important. The binding energy can be known from the mass of double hypernucleus. The mass can be reconstructed by the kinetic energies which are converted from the ranges of decay daughter nucleus with the help of RE relation.

Therefore, the calibration of the density of emulsion layer in each emulsion sheet is necessary for the RE relation. Alpha decay track which have monochromatic kinetic energy of 8.785 MeV from ^{212}Po from the natural radioisotopes of the thorium series have been used to calibrate the density of emulsion layer. The statistical and systematic energy errors which generated from the density of emulsion layer is very important to get optimal RE relation.

The statistical error was investigated by deciding the suitable number of alpha decay tracks for the density calibration using ~1500 alpha decay tracks ^{212}Po. The sufficient number of alpha tracks was determined to be at least 150 alpha tracks. The ratio of kinetic energy error from range straggling and emulsion density error was also calculated. The kinetic energy error from range straggling is one order magnitude larger than that of density error.

The systematic energy error was calibrated using the densities from alpha decay track from ^{212}Po, ^{214}Po, and ^{226}Ra for different energy regions. The density was calibrated from the ranges of 49.21 μm, 40.12 μm and 20.13 μm, with their respective energies. The largest systematic error between 20 μm and 50 μm was found to be about 25 keV. Moreover, we tried to calibrate the systematic error in the higher energy region by using the range of ${}^{5}_{\Lambda}$He (~90 μm) from IBUKI event. It was found that the systematic energy error ~90 μm is 22keV. The systematic energy error from the density calibration is 1/10 of the error in the mass reconstruction of the IBUKI event. The result is

significantly smaller than the measurement error and shows that the accuracy of the calibration method with alpha particles is reasonable to apply hypernuclear events analysis.

This study claimed about the statistical and systematic energy error in RE relation related to the density of emulsion layer. It is very important for the future analysis scheme of double hypernuclear event to provide a reasonable energy error.

Acknowledgments

I would like to express my deepest appreciation to all the people who worked together, provided advice, supported, and encouraged me towards the attainment of a doctorate degree. In particular, I would like to express sincere thanks to my supervisor, Professor Kazuma NAKAZAWA, for the valuable advice and instruction on my graduate studies, starting from master's all the way to Ph. D research, for his motivation, enthusiasm, and immense knowledge. His guidance helped me in all aspects of graduate studies and research.

I also wish to thank Dr. Masahiro Yoshimoto for his help, guidance, and teaching, hardware, software and other technical support for my research work. My sincere thanks also go to Dr. Junya Yoshida and Mr. Ayumi Kasagi, for their help, patience, advice, and encouragement when I am carrying the research work and my thesis.

I would like to thank the AGP program for providing financial support for my graduate studies and catering for my living expenses in Japan. Special appreciation to IUCHI scholarship for supplementing daily living expenses through monthly stipends.

I am deeply grateful to my senior Dr. Aung Nay Lin Nyaw for the support, explanation of varying concepts, data analysis and general life support in my Ph.D journey. You have been a true elder brother indeed. Sincere thanks to all friends in Gifu University who made living in Gifu a fun and memorable experience. Zaw Minh Han, Noe Noe, Go Sian, etc. You guys all assisted me in ways I cannot express.

I would like to express my special gratitude to Dr. Muguro Joseph Kamau for encouraging me to be the best in all I do and thank you for being patient and for being so kind to me.

Finally, I would address my heartfelt gratitude to my family who encouraged me and prayed for me throughout the time of my research. Your sacrifice and loving attitude have kept me going.

References

[1] M. Danysz & J. Pinewski, Philos. Mag. 44, 348 (1953).

[2] Debarati Chatterjee & Isaac Vidaña, Eur. Phys. J. A, 52, 29 (2016).

[3] M. Danysz et al., Phys. Rev. Lett. 11, 29 (1963).

[4] S. Aoki, et al., Nucl. Phys. A 828, 191 (2009).

[5] S. Aoki, et al., Prog. Theor. Phys. 85, 1287 (1991).

[6] J. K. Ahn et al., Phys. Rev. C88, 014003 (2013).

[7] K. Nakazawa et al., Prog. Theor. Exp. Phys. 2015, 033D02 (2015).

[8] E. Hiyama and K. Nakazawa, Annu. Rev. Nucl. Part. Sci. 68:131-59 (2018).

[9] K. Sasaki et al., Nucl. Phys. A998, 121737 (2020)

[10] H. Ito et al., JPS Conf. Proc. 8, 021007 (2015).

[11] K. Imai, K. Nakazawa, H. Tamura, J-PARC E07 Proposal

[12] C.M.G. Lattes, G.P.S. Occhialini, C.F. Powell, Nature 160:456 (1947).

[13] S. Hayakawa, Ph. D. Thesis, Osaka University, unpublished (2019).

[14] H. Ekawa et al., Prog. Theor. Exp. Phys. 2019, 021D02(2019).

[15] A. N. L. Nyaw, et al., Bull. Soc. Photogr. Imag. Jpn., 30, 22 (2020).

[16] S. Hayakawa, et al., Phys. Rev. Lett. 126 062501 (2021).

[17] M. Yoshimoto, et al., Prog. Theor. Exp. Phys., 2021, 073D02 (2021).

[18] H. H. Heckman, B. L. Perkins, W.G Simon, F. M. Smith, W. H. Barkas, Phys. Rev., 117, 544 (1960).

[19] W. H. Barkas, P. H. Parrett, P. Cüer, H. H. Heckman, Nuovo Cimento, 8, 185 (1958).

[20] W. H. Barkas, F. M. Smith, W. Birnbaum, Phys. Rev., 98, 605 (1955).

[21] G. P. S. Occhialini and C. F. Powell, Nature, 159, 93 (1947)

[22] J. Yoshida, et al., Nuclear Inst. Meth. Phys. Res. A, 847, 86 (2017).

[23] J. Yoshida, et al., Nuclear Inst. Meth. Phys. Res. A, 989, 164930 (2021).

[24] M. Buda, et al., A systematic study of the class imbalance problem in convolutional neural networks, CoPR abs/1710.05381. arXiv:1710.05381. URL http://arxiv.org/abs/1710.05381.

[25] https://github.com/ufoym/imbalanced-dataset-sampler.

[26] E.D. Cubuk, et al., Randaugment: Practical automated data augmentation with a reduced search space, 2019, arXiv:1909.13719.

[27] https://github.com/ildoonet/pytorch-randaugment.

[28] D.P. Kingma, J. Ba, Adam: A method for stochastic optimization, 2014, arXiv:
1412.6980.

[29] J. Davis, M. Goadrich, The relationship between precision-recall and ROC curves, in: Proceedings of the 23rd International Conference on Machine Learning, ICML '06, Association for Computing Machinery, New York, NY, USA, 2006, pp. 233–240, http://dx.doi.org/10.1145/1143844.1143874.

[30] P. M. Lin, et al., Bull. Soc. Photogr. Imag. Jpn., 32, 10 (2022)